Article

Cell

Omega-3 Fatty Acids Activate Ciliary FFAR4 to Control Adipogenesis

Graphical Abstract

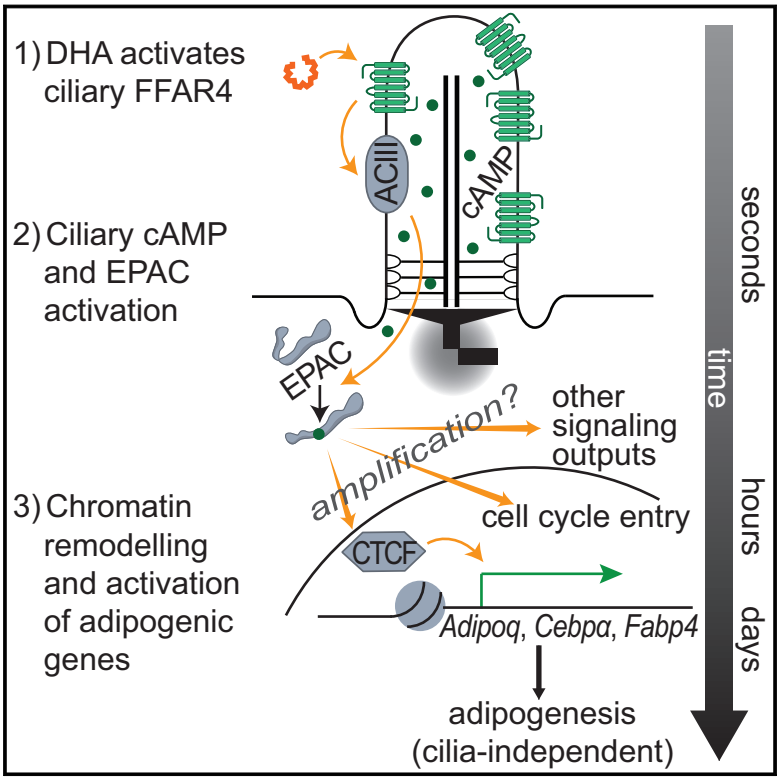

Authors

Keren I. Hilgendorf, Carl T. Johnson, Anja Mezger, ..., Jeremy F. Reiter, Daniel Kopinke, Peter K. Jackson

Correspondence

jeremy.reiter@ucsf.edu (J.F.R.), dkopinke@ufl.edu (D.K.), pjackson@stanford.edu (P.K.J.)

In Brief

An omega-3 fatty acid drives adipogenesis through ciliary signaling.

Highlights

- Preadipocytes, located along blood vessels, are ciliated *in vitro* and *in vivo*
- Loss of preadipocyte ciliation strongly impairs white adipose tissue expansion
- Ciliary GPCRs are critical for adipogenesis, and FFAR4/GPR120 localizes to cilia
- ω-3 fatty acids activate ciliary FFAR4 and trigger adipogenesis via ciliary cAMP

Hilgendorf et al., 2019, Cell *179*, 1289–1305
November 27, 2019
https://doi.org/10.1016/j.cell.2019.11.005

CellPress

Cell

Omega-3 Fatty Acids Activate Ciliary FFAR4 to Control Adipogenesis

Keren I. Hilgendorf,[1] Carl T. Johnson,[1,2] Anja Mezger,[3,4,10] Selena L. Rice,[5] Alessandra M. Norris,[6] Janos Demeter,[1] William J. Greenleaf,[3,7,8] Jeremy F. Reiter,[5,7,*] Daniel Kopinke,[5,11,*] and Peter K. Jackson[1,9,12,*]

[1]Baxter Laboratory, Department of Microbiology & Immunology, Stanford University School of Medicine, Stanford, CA 94305, USA
[2]Department of Medicine, Stem Cell and Regenerative Medicine Program, Stanford University School of Medicine, Stanford, CA 94305, USA
[3]Department of Genetics, Stanford University, Stanford, CA 94305, USA
[4]Department of Medical Biochemistry and Biophysics, Karolinska Institutet, 17177 Stockholm, Sweden
[5]Department of Biochemistry and Biophysics, Cardiovascular Research Institute, University of California, San Francisco, San Francisco, CA, USA
[6]Department of Pharmacology and Therapeutics, University of Florida, Gainesville, FL 32610, USA
[7]Chan Zuckerberg Biohub, San Francisco, CA 94158, USA
[8]Department of Applied Physics, Stanford University, Stanford, CA 94305, USA
[9]Department of Pathology, Stanford University School of Medicine, Stanford, CA 94305, USA
[10]Present address: Discovery Biology, Discovery Sciences, BioPharmaceuticals R&D, AstraZeneca, Gothenburg, Sweden
[11]Present address: Department of Pharmacology and Therapeutics, University of Florida, Gainesville, FL 32610, USA
[12]Lead Contact
*Correspondence: jeremy.reiter@ucsf.edu (J.F.R.), dkopinke@ufl.edu (D.K.), pjackson@stanford.edu (P.K.J.)
https://doi.org/10.1016/j.cell.2019.11.005

SUMMARY

Adult mesenchymal stem cells, including preadipocytes, possess a cellular sensory organelle called the primary cilium. Ciliated preadipocytes abundantly populate perivascular compartments in fat and are activated by a high-fat diet. Here, we sought to understand whether preadipocytes use their cilia to sense and respond to external cues to remodel white adipose tissue. Abolishing preadipocyte cilia in mice severely impairs white adipose tissue expansion. We discover that TULP3-dependent ciliary localization of the omega-3 fatty acid receptor FFAR4/GPR120 promotes adipogenesis. FFAR4 agonists and ω-3 fatty acids, but not saturated fatty acids, trigger mitosis and adipogenesis by rapidly activating cAMP production inside cilia. Ciliary cAMP activates EPAC signaling, CTCF-dependent chromatin remodeling, and transcriptional activation of PPARγ and CEBPα to initiate adipogenesis. We propose that dietary ω-3 fatty acids selectively drive expansion of adipocyte numbers to produce new fat cells and store saturated fatty acids, enabling homeostasis of healthy fat tissue.

INTRODUCTION

Mesenchymal stem and progenitor cells divide to support homeostasis and expansion of four major tissues: muscle, bone, cartilage, and fat. The signals that regulate mesenchymal tissue regeneration and expansion remain unclear, including (1) how growth factors and nutritive fluxes trigger cell cycle entry and stem cell expansion; (2) what structures in tissue anchor and organize the stem cell niche; and (3) what epigenetic programs favor stem cell maintenance versus differentiation.

White adipose tissue (WAT) stores energy and controls energy homeostasis (Rosen and Spiegelman, 2014). WAT can regenerate, expand, and contract in response to tissue damage or altered nutritional flux (Sakaguchi et al., 2017). Specifically, WAT can expand by both generating more adipocytes (hyperplasia) and by storing more fat in existing adipocytes (hypertrophy) (Haczeyni et al., 2018). Excessive hypertrophy is linked to increased tissue hypoxia, fibrosis, and inflammation, leading to insulin resistance and metabolic dysfunction (Ghaben and Scherer, 2019). The adipogenic potential of preadipocytes affects the balance between hypertrophic and hyperplastic WAT expansion and is influenced by age, sex, location of WAT depots, genetic predisposition, and nutritional fluxes (Arner et al., 2013; Jeffery et al., 2016; Karastergiou and Fried, 2017; Palmer and Kirkland, 2016).

Adipogenesis is regulated by a combination of signals including insulin and cyclic AMP (cAMP). In response to adipogenic signals, preadipocytes both *in vitro* and *in vivo* exit quiescence and re-enter the cell cycle to regenerate preadipocytes and generate daughter cells that differentiate into adipocytes (Jeffery et al., 2015; Wang et al., 2013). The molecular mechanism of adipogenesis has been characterized extensively in a murine cell line, 3T3-L1 cells. In response to the differentiation factors insulin, the glucocorticoid dexamethasone (Dex), and the cAMP elevating drug IBMX, 3T3-L1 cells re-enter the cell cycle and activate an adipogenic transcriptional cascade involving PPARγ and CEBPα (Rosen et al., 2000; Tang et al., 2003). Apart from insulin, the physiological factors that promote adipogenesis *in vivo* remain unclear. Discovering factors that shift the balance of WAT expansion to hyperplasia could provide a new therapeutic strategy for limiting the consequences of obesity.

Preadipocytes reside along the vasculature in fat tissue, where they may sense systemic changes in metabolites and couple

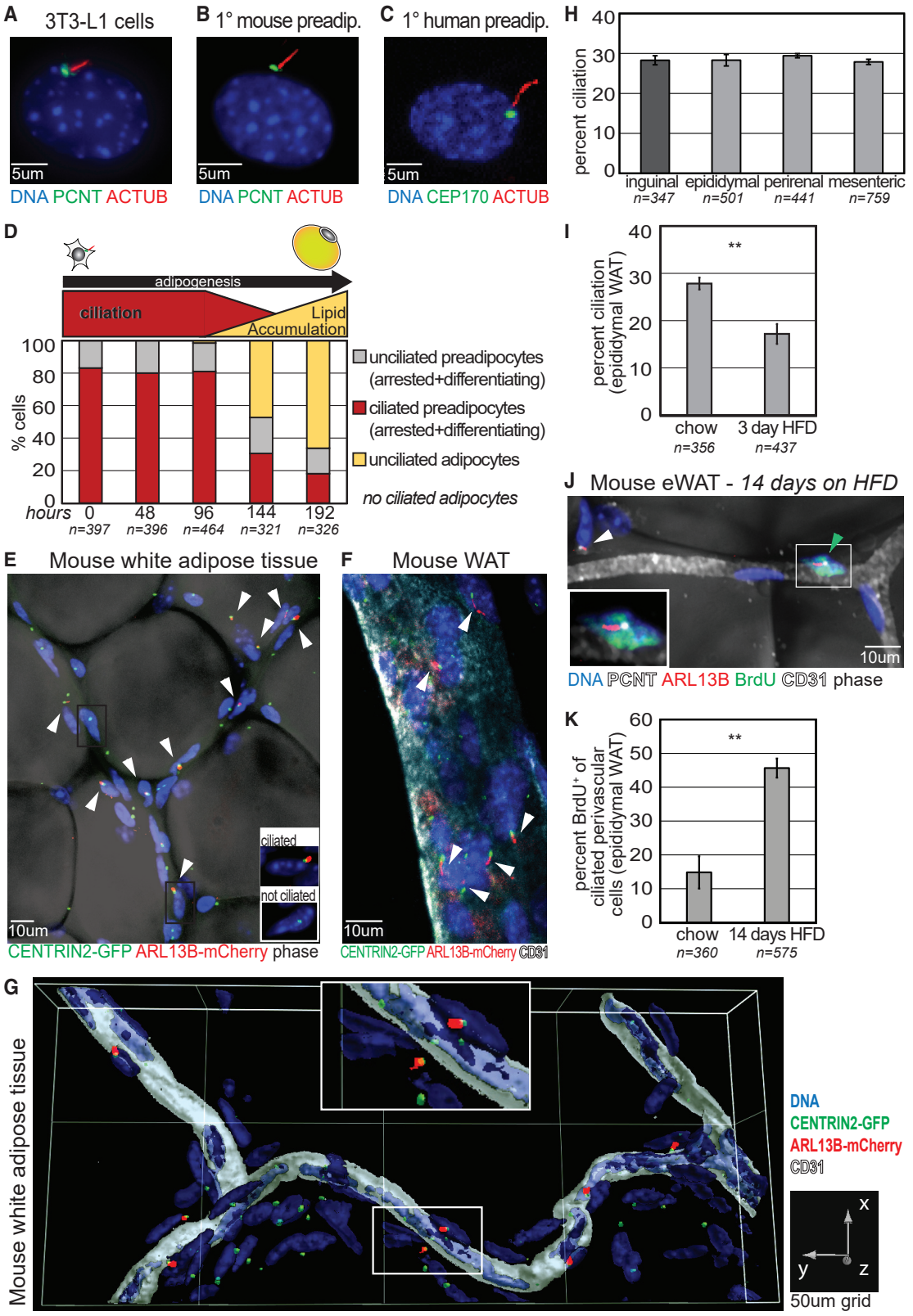

(legend on next page)

nutritional fluxes to adipogenesis (Tang et al., 2008). Earlier studies lack definitive markers and functional identity to visualize the preadipocyte in fat tissue, although we and others have noted that preadipocytes, like other quiescent mesenchymal stem and progenitor cells, possess a single projection called a primary cilium (Kopinke et al., 2017; Lyu and Zhou, 2017; Tummala et al., 2010).

The primary cilium is a sensory organelle nucleated by the mother centriole and enriched with receptors, particularly G protein-coupled receptors (GPCRs) (Hilgendorf et al., 2016). Transport of these receptors into the cilium is regulated by at least two protein complexes, the BBSome and the TULP3-IFTA complex (Mukhopadhyay et al., 2010; Nachury et al., 2007). Recent studies have reported the potential importance of primary cilia for differentiation into adipocytes (Forcioli-Conti et al., 2015; Huang-Doran and Semple, 2010; Marion et al., 2012; Marion et al., 2009; Qiu et al., 2010; Zhu et al., 2009), osteocytes (Xiao and Quarles, 2010; Yuan and Yang, 2016), chondrocytes (Deren et al., 2016; Kelly and Jacobs, 2010), and myocytes (Fu et al., 2014; Jaafar Marican et al., 2016). The importance of primary cilia for mesenchymal stem and progenitor cell function is highlighted by human genetic disorders called ciliopathies caused by ciliary dysfunction. Some ciliopathies are characterized by tissue degeneration and metabolic dysfunctions including obesity and diabetes (Hildebrandt et al., 2011; Waters and Beales, 2011).

To discover how fat tissue organizes potential ciliated progenitor cells, we used a transgenic mouse model with fluorescently tagged primary cilia. We found that an extensive population of ciliated cells is localized along the vasculature in fat pads, positioning these cells to sense and respond to systemic fluxes of metabolites and growth factors. To determine whether preadipocytes use their cilia to sense these factors, we genetically removed preadipocyte cilia and found that ciliation of preadipocytes is critically important for WAT expansion. To discover key fluxes that trigger differentiation, we screened for ciliary GPCRs as candidate adipogenic regulators, and we discovered that FFAR4/GPR120 localizes to preadipocyte cilia *in vitro* and *in vivo*. The FFAR4/GPR120 ligand DHA, an ω-3 fatty acid, but not saturated fatty acids, efficiently induces adipogenesis. Addition of DHA or synthetic FFAR4 agonists to preadipocytes triggers a rapid increase in ciliary cAMP and activation of the cAMP effector EPAC critical for adipogenesis. Profiling of DHA/FFAR4-dependent transcriptional and chromatin-remodeling activities showed that the regulator of chromatin architecture CTCF helps activate transcriptional effectors including CEBPα to promote adipogenesis. Thus, our results reveal that preadipocyte cilia selectively sense ω-3 fatty acids through FFAR4 to induce adipogenesis.

RESULTS

Characterizing the Primary Cilium of Preadipocytes *In Vitro* and *In Vivo*

Previous studies have shown that human and murine preadipocytes are ciliated *in vitro* when quiescent and that the primary cilium is important for adipogenesis, in part by displaying a highly sensitized IGF-1 receptor (Zhu et al., 2009). To confirm and extend these observations, we first assessed the ciliation status of differentiating 3T3-L1 cells. 80% of confluent 3T3-L1 cells are ciliated, and primary cilia are uniformly lost as differentiating 3T3-L1 cells accumulate lipid (Figures 1A and 1D). While 3T3-L1 cells in the early phase of differentiation with little or no lipid are typically ciliated, mature, lipid-laden 3T3-L1 adipocytes are not ciliated, suggesting that the primary cilium specifically functions in undifferentiated and differentiating preadipocytes. Similarly, both mouse and human preadipocytes grown to confluency are ciliated, and the primary cilium is lost during differentiation (Figures 1B, 1C, and S1A). Specifically, 80% of FACS-sorted mouse preadipocytes (Lin^- $CD34^+$ $CD29^+$ $SCA1^+$) are ciliated. This cell population has previously been shown to be capable of efficient *in vitro* differentiation and reconstitution of WAT depots in lipodystrophic mice (Rodeheffer et al., 2008). These findings suggest that the primary cilium may be a functional marker of preadipocytes *in vivo*.

To test this hypothesis, we visualized ciliated cells within intact fat tissue. Of note, there has been considerable progress in identifying *in vivo* markers of preadipocytes, including PDGFRα for lineage tracing and sorting, but to date, no unique, specific *in vivo* preadipocyte markers have been identified (Berry and Rodeheffer, 2013; Guimaraes-Camboa et al., 2017; Gupta et al., 2012; Hepler et al., 2017; Jiang et al., 2014; Rodeheffer et al., 2008; Vishvanath et al., 2016). Functional studies suggested that preadipocytes reside along the vasculature within WAT (Tang et al., 2008). We used a transgenic mouse model

Figure 1. Preadipocytes Are Ciliated *In Vitro* and *In Vivo* and an Abundant Perivascular Cell in Fat Tissue

(A–C) Immunofluorescence staining visualizes primary cilia on (A) confluent 3T3-L1 cells, (B) primary mouse preadipocytes (Lin^-, $CD34^+$, $SCA1^+$, $CD29^+$), and (C) human preadipocytes; DAPI stains nuclei. ACTUB stains axoneme; PCNT and CEP170 stain the basal body.

(D) The primary cilium is lost in differentiating 3T3-L1 cells. n, number of cells counted.

(E–G) Whole-mount imaging of epididymal WAT from *cilia glow* mouse identifies ciliated perivascular cells. All cells have a CENTRIN2-GFP+ centrosome; ciliated cells are CENTRIN2-GFP+ and ARL13B-mCherry+ (inset). (E) Lipid droplets are visualized by phase and (F) blood vessels are CD31+. (G) 3D surface reconstruction of blood vessel and adjacent ciliated perivascular cells.

(H) Quantification of ciliation on perivascular cells in subcutaneous (dark gray) and visceral (light gray) mouse WAT of *cilia glow* mice. Bar graphs show average from 2 littermates ± SD. n, number of perivascular ciliated cells counted.

(I) HFD promotes transient deciliation in epididymal WAT of *cilia glow* mice after 3 days. Bar graph shows average of 4 independent experiments ±SEM, each using 1–2 littermates per diet. n, number of perivascular cells counted; p value calculated using chi-square test is $p < 0.005$.

(J and K) 2 weeks of HFD activates ciliated perivascular cells to re-enter the cell cycle. (J) Whole-mount image and (K) quantification of BrdU+ ciliated perivascular cells in epididymal WAT.

Data are percent BrdU+ of ciliated perivascular cells (n = 3 mice on HFD; n = 2 mice on chow) ± SEM. n, number of perivascular ciliated cells counted. Arrowheads point to perivascular ciliated cells. p values calculated using t test unless noted otherwise, $^{**}p < 0.01$. All images acquired using a 40× oil objective, with the exception of C, for which a 20× air objective was used. See also Figure S1.

expressing fluorescently tagged CENTRIN2 and ARL13B to visualize the base and axoneme of primary cilia, respectively (henceforth referred to as *cilia glow* mice). Strikingly, ciliated cells within fat pads are organized along vascular tracts, and mature adipocytes are not ciliated (Figure 1E). The expansive populations of ciliated cells are located immediately adjacent to blood vessels (Figures 1F, 1G, and S1B). Ciliated perivascular cells account for ~30% of all perivascular cells in both visceral and subcutaneous WAT (Figure 1H). Staining and quantifying cilia in non-transgenic mice verifies the proportion of ciliated perivascular cells in WAT (Figure S1C). Macrophages, which can account for up to 40% of other cells in WAT (Weisberg et al., 2003), are not ciliated (Figure S1D). As further confirmation, we genetically marked preadipocytes using a tamoxifen-inducible *Pdgfrα*-CreERT allele (Kang et al., 2010) crossed to a Rosa26^{EYFP} reporter (Srinivas et al., 2001). PDGFRα-lineage perivascular cells in murine WAT are ciliated *in vivo* (Figure S1E). Thus, we propose that the primary cilium marks the resident preadipocyte population along the vasculature *in vivo*, raising the hypothesis that ligands carried by circulation can activate these precursor cells to differentiate.

To test this hypothesis, we activated preadipocytes *in vivo* using a high-fat diet (HFD). Previously, HFD was shown to induce quiescent preadipocytes in visceral WAT to rapidly re-enter the cell cycle after 3 days and then exit the cell cycle after 1 week (Jeffery et al., 2015). Of note, cells transiently lose their cilia during mitosis (Ford et al., 2018; Kim and Dynlacht, 2013). Consistent with the hypothesis, there is a transient decrease in the percentage of ciliated perivascular cells after 3 days on an HFD (Figure 1I). After 2 weeks on an HFD, we assessed ciliation and BrdU incorporation and found that 50% of all ciliated perivascular cells were BrdU+, indicating that they were activated in response to the HFD to enter the adipogenic program (Figures 1J and 1K). Taken together, the primary cilium marks preadipocytes that are responsive to dietary fatty acids *in vivo*.

Preadipocyte Cilia Are Critical for WAT Expansion *In Vivo*

To assess the *in vivo* function of preadipocyte cilia, we conditionally deleted *Ift88*, a gene required for ciliogenesis and ciliary maintenance, in preadipocytes using tamoxifen-inducible *Pdgfrα*-CreERT. We refer to *Pdgfrα*-CreERT *Ift88*$^{flox/-}$ mice treated with tamoxifen hereafter as PA$^{no\ cilia}$ mice. Control mice were tamoxifen-treated littermates lacking *Pdgfrα*-CreERT (*Ift88*$^{flox/-}$) or retaining one wild-type allele of *Ift88* (*Pdgfrα*-CreERT *Ift88*$^{flox/+}$) (Figure 2A). Preadipocytes of PA$^{no\ cilia}$ mice treated with tamoxifen at 3 weeks of age lacked cilia (Figure S2A). Notably, loss of preadipocyte cilia dramatically reduced body weight, with both PA$^{no\ cilia}$ male and female mice weighing almost 20 g less than control male and female littermates at 17 weeks post-tamoxifen administration (Figure 2A). Echo-MRI measurement revealed that this weight loss was largely due to reduced total fat mass (Figure 2B). Loss of cilia in preadipocytes resulted in a significant reduction of gonadal WAT (Figure 2B). We observed similar, but quantitatively smaller, differences in body weight and fat mass when tamoxifen was administered at 6 weeks of age, arguing that preadipocyte cilia are continuously required for full WAT expansion (Figure S2B).

Consistent with reduced fat mass, histological analysis showed that the average adipocyte is smaller in PA$^{no\ cilia}$ mice (Figure S2C). As expected, serum leptin levels are also reduced in PA$^{no\ cilia}$ mice (Figure 2C). Since preadipocytes, but not mature adipocytes, are ciliated (Figures 1D and 1E), we hypothesized that cilia are critical for the adipogenic potential of preadipocytes, accounting for the decreased WAT expansion in PA$^{no\ cilia}$ mice. To test this hypothesis, we introduced the *Rosa26*^{EYFP} reporter into our control (*Pdgfrα-CreERT Ift88*$^{flox/+}$ *Rosa26*^{EYFP}, referred to hereafter as control^{lineage}) and PA$^{no\ cilia}$ (*Pdgfrα-CreERT Ift88*$^{flox/-}$ *Rosa26*^{EYFP}, referred to hereafter as PA$^{no\ cilia+lineage}$) mice, and we followed the fate of preadipocytes with and without cilia by virtue of EYFP expression. Specifically, we quantified lineage-traced, EYFP^{+} adipocytes in PA$^{no\ cilia+lineage}$ and control^{lineage} mice. Deletion of cilia in preadipocytes dramatically reduced the proportion of EYFP-expressing differentiated adipocytes (Figure 2D). Thus, preadipocyte cilia are important for adipogenesis and WAT expansion.

Despite the reduction in total fat mass in PA$^{no\ cilia}$ mice, we did not note symptoms of lipodystrophy, such as increased serum free fatty acid, insulin, or glucose levels, or hepatic fat deposition in PA$^{no\ cilia}$ mice (Figures S2D and S2E). We do not know if these hallmarks of lipodystrophy would become apparent with age or if PA$^{no\ cilia}$ mice were challenged with an HFD.

We also interrogated other tissues to assess potential effects on WAT expansion. Pdgfrα-CreERT is active in WAT (Figure S1E) and does not induce extensive recombination in the liver, pancreas, or small or large intestine (O'Rourke et al., 2016). Within skeletal muscle, the activity of this transgenic Pdgfrα-CreERT allele is restricted to *Pdgfrα*-expressing fibro-adipogenic progenitors (Kopinke et al., 2017). As primary cilia in the brain have previously been shown to regulate satiety and locomotion (Davenport et al., 2007; Loktev and Jackson, 2013; Siljee et al., 2018), we assessed PA$^{no\ cilia}$ and control mice for food intake, energy expenditure, or activity using the comprehensive lab animal monitoring system (CLAMS) and observed no differences (Figure S2F). We also did not observe changes in the amount of gross brown adipose tissue in PA$^{no\ cilia}$ mice (Figure S2G). It would be interesting to test for a role of preadipocyte cilia during β3-adrenergic induced *de novo* BAT formation. To assess whether differences in energy absorption might contribute to the reduction in fat mass, we evaluated levels of glucose and free fatty acids in serum or adaptive hyperphagia (Crenn et al., 2004), but we found no differences between control and PA$^{no\ cilia}$ mice (Figures S2E and S2F). We therefore conclude that preadipocyte ciliation is important for WAT expansion and that preadipocyte cilia promote adipogenesis *in vivo*.

TULP3, an Essential Regulator of Ciliary GPCR Entry, Is Critical for Adipogenesis

To assess how primary cilia promote adipogenesis, we focused on identifying GPCRs, the largest class of ciliary receptors (Hilgendorf et al., 2016), and hypothesized that preadipocyte ciliary GPCRs transduce adipogenic cues. To test this dependence, we used CRISPR-Cas9 to generate 3T3-L1 cells lacking TULP3, a protein required for transporting GPCRs into the primary cilium (Figures 3A and S3A) (Loktev and Jackson, 2013; Mukhopadhyay et al., 2010). 3T3-L1 cells lacking TULP3 form primary cilia

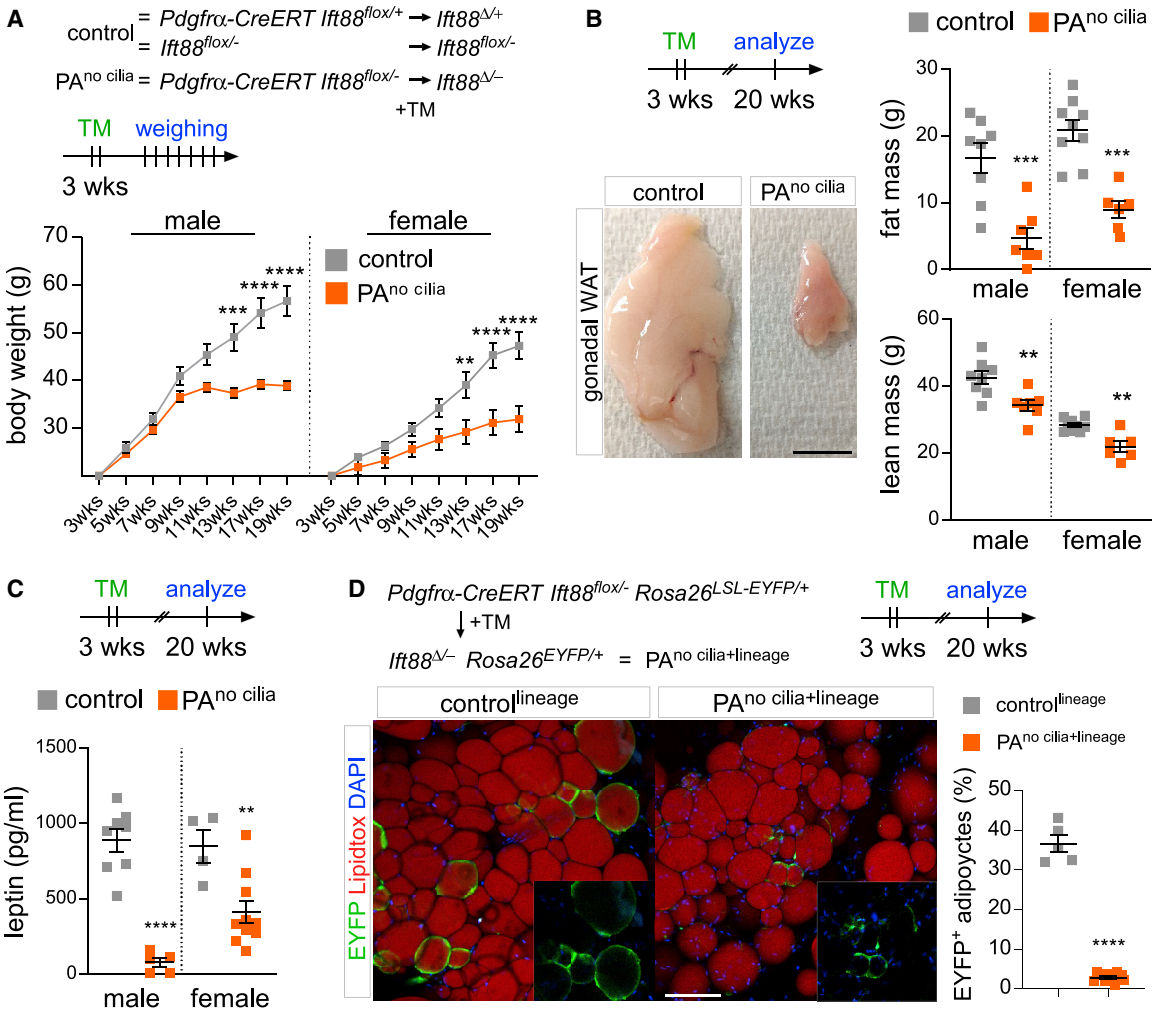

Figure 2. Preadipocyte Cilia Promote WAT Expansion

(A) Body weight measurements of control (*Ift88*$^{flox/-}$ and *Pdgfrα-CreERT Ift88*$^{\Delta/+}$) and PA$^{no\ cilia}$ mice (*Pdgfrα-CreERT Ift88*$^{\Delta/-}$) (n = 5 per sex and genotype).

(B) Dissected gonadal fat pads and measurements of total fat and lean mass by Echo-MRI of control and PA$^{no\ cilia}$ mice 17 weeks after tamoxifen administration. Scale bar, 1 cm.

(C) Serum leptin levels of control and PA$^{no\ cilia}$ mice 17 weeks after tamoxifen administration.

(D) Immunofluorescence staining for lineage marker (EYFP, green) and adipocytes (LipidTox, red) of 20-week-old control^{lineage} (*Pdgfrα-CreERT Ift88*$^{\Delta/+}$ *Rosa26*^{EYFP}) and PA$^{no\ cilia+lineage}$ (*Pdgfrα-CreERT Ift88*$^{\Delta/-}$ *Rosa26*^{EYFP}) mice after tamoxifen administration at 3 weeks of age. PA$^{no\ cilia+lineage}$ mice contain fewer lineage-derived EYFP^{+} adipocytes compared to control^{lineage} mice. Scale bar, 100 μm.

All data are represented as mean ± SEM. p values calculated using standard t test and two-way ANOVA followed by Tukey's multiple comparison test (**<0.01, ***<0.001, and ****<0.0001). See also Figure S2.

at the expected frequency, but they lack a ciliary protein (ARL13B), consistent with published reports (Figure S3C) (Hwang et al., 2019). We assessed adipogenesis by oil red O staining, quantified by absorbance of isopropanol extracted dye. Intriguingly, loss of TULP3 did not attenuate adipogenesis of 3T3-L1 cells treated with the full complement of the standard, historical differentiation factors (Figure 3B). This differentiation media (DM) includes a high concentration of Dex, a glucocorticoid receptor agonist that directly and broadly promotes transcription (Siersbæk et al., 2012), and thus may uncouple adipogenesis from the sensing of extracellular cues by GPCRs. Therefore, we titrated down the historical DM, which only slightly decreased the efficiency and kinetics of 3T3-L1 adipogenesis at 0.5 or 0.25× concentrations. Importantly, TULP3 was required for efficient adipogenesis using this more dilute DM, as shown by sgRNA knockout (Figure 3B) or siRNA knockdown of *Tulp3* (Figures S3D–S3F). This loss of adipogenic activity following *Tulp3* depletion was rescued by expression of human *TULP3*, confirming the specificity of the effect (Figures 3C, 3D, and S3G).

Overexpression of *TULP3* in wild-type 3T3-L1 preadipocytes increased the rate and the amount of adipogenesis, as assessed by kinetic analysis of fluorescence intensity of the lipophilic green fluorescent dye BODIPY (Figure 3D). This experiment indicates that TULP3 levels may determine signaling efficiency and

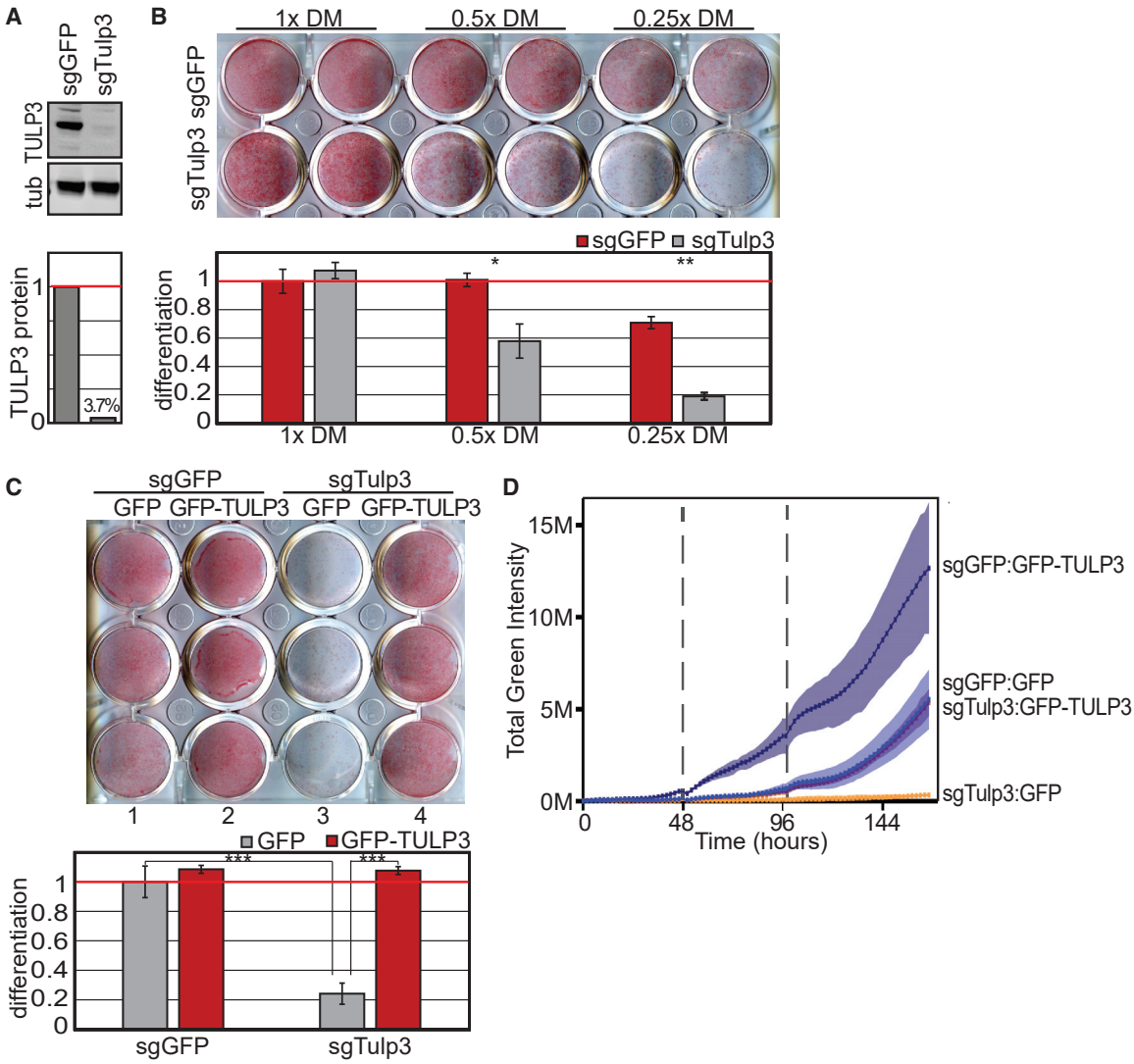

Figure 3. TULP3 Knockouts Support a Requirement for Ciliary GPCRs during Adipogenesis

(A) Immunoblot showing depletion of TULP3 protein in 3T3-L1 cells.

(B) TULP3 is required for 3T3-L1 differentiation induced by reduced amounts of DM. Lipids are visualized by oil red O staining (top) and quantified by measuring absorbance post-isopropanol extraction of oil red O (bottom).

(C) Loss of adipogenic potential due to TULP3 depletion is rescued by human GFP-tagged TULP3.

(D) TULP3 expression levels correlate with adipogenic potential as determined by live imaging and quantification of green fluorescence intensity using BODIPY. Dotted line denotes media change. Shaded area describes 95% confidence interval. Bar graphs are normalized mean ± SD; *p < 0.05; **p < 0.01; ***p < 0.001. See also Figure S3.

outcome. Thus, *TULP3* expression levels, and, by extension, ciliary receptor trafficking, may accelerate adipogenesis in 3T3-L1 cells.

Preadipocytes Display FFAR4 in the Primary Cilium

Next, we sought to discover which GPCRs may function at preadipocyte primary cilia. We compiled a list of candidate ciliary preadipocyte GPCRs, based on expression patterns and receptors with a known role in regulating adipogenesis (Table S1). These GPCRs were expressed as C-terminally tagged GFP fusion proteins and screened for ciliary localization in 3T3-L1 preadipocytes (Figure 4A). This analysis uncovered the free fatty acid receptor FFAR4/GPR120 as distinctively ciliary (Figure S4A).

To confirm ciliary localization of FFAR4, we generated an antibody against the protein. Notably, endogenous FFAR4 localized to the primary cilium of undifferentiated, confluent 3T3-L1 preadipocytes as well as to the primary cilium of primary preadipocytes isolated from mouse and human WAT (Figures 4B–4D and S4B). Moreover, FFAR4 also localized to the primary cilium of perivascular ciliated preadipocytes *in vivo* (Figure 4E). We confirmed the specificity of staining in 3T3-L1 cells lacking

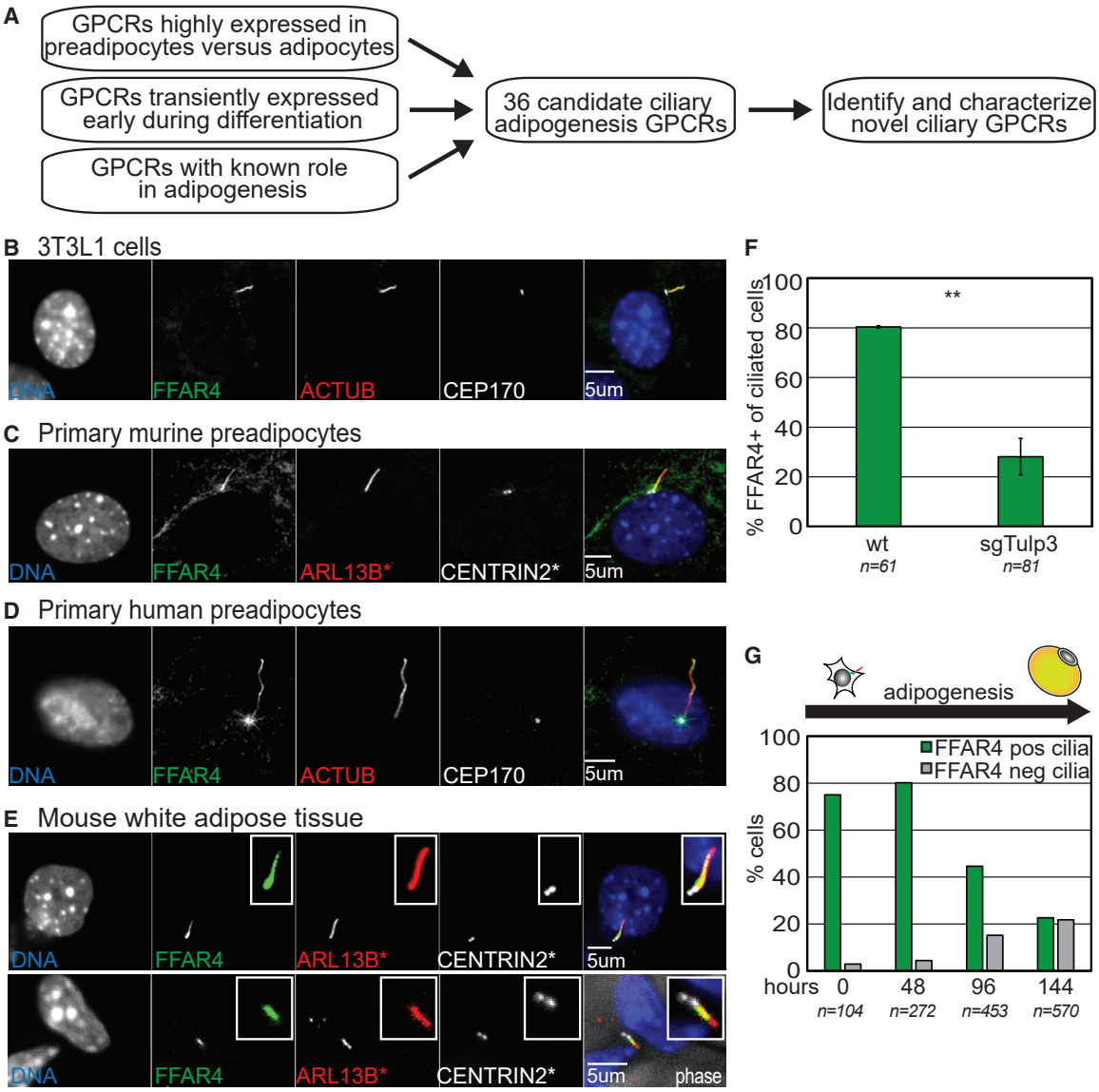

Figure 4. FFAR4 Is a Ciliary GPCR Displayed by Preadipocytes

(A) Schematic of screen to identify ciliary GPCR in 3T3-L1 cells.

(B–D) Endogenous FFAR4 localizes to the primary cilium of undifferentiated, confluent (B) 3T3-L1 cells, (C) primary mouse preadipocytes in the stromal vascular fraction (SVF, depleted for RBCs and WBCs) from *cilia glow* mice, and (D) primary human preadipocytes.

(E) Whole-mount images of epididymal WAT from *cilia glow* mice show that ciliated perivascular cells display ciliary FFAR4.

(F) Loss of TULP3 prevents ciliary trafficking of FFAR4 in 3T3-L1 preadipocytes.

(G) Induction of differentiation results in internalization of ciliary FFAR4.

n, number of cells counted; bar graph is average ± SD; **p < 0.01. (B)–(D) acquired using a 40× oil objective; (E) acquired using 63× oil objective. See also Figure S4.

FFAR4 and in mouse primary preadipocytes isolated from *Ffar4* knockout mice (Figures S4C–S4E). Finally, ciliary FFAR4 localization is TULP3 dependent (Figures 4F and S4F).

To better understand how FFAR4 might participate in adipogenesis, we assessed the expression and localization of FFAR4 during adipogenesis. Intriguingly, and consistent with previous observations, overall FFAR4 mRNA and protein levels increased dramatically during adipogenesis and as the primary cilium is lost (Figure S4G) (Gotoh et al., 2007). FFAR4 is at low levels in undifferentiated cells, except for the distinctive pool in the cilium. Moreover, FFAR4 relocalized from primary cilia to the plasma membrane as 3T3-L1 cells underwent differentiation (Figures 4G and S4H). Thus, we propose that FFAR4 can localize to both the primary cilium and the plasma membrane and that FFAR4 has a higher efficiency for ciliary targeting such that it specifically localizes to primary cilia of undifferentiated, ciliated

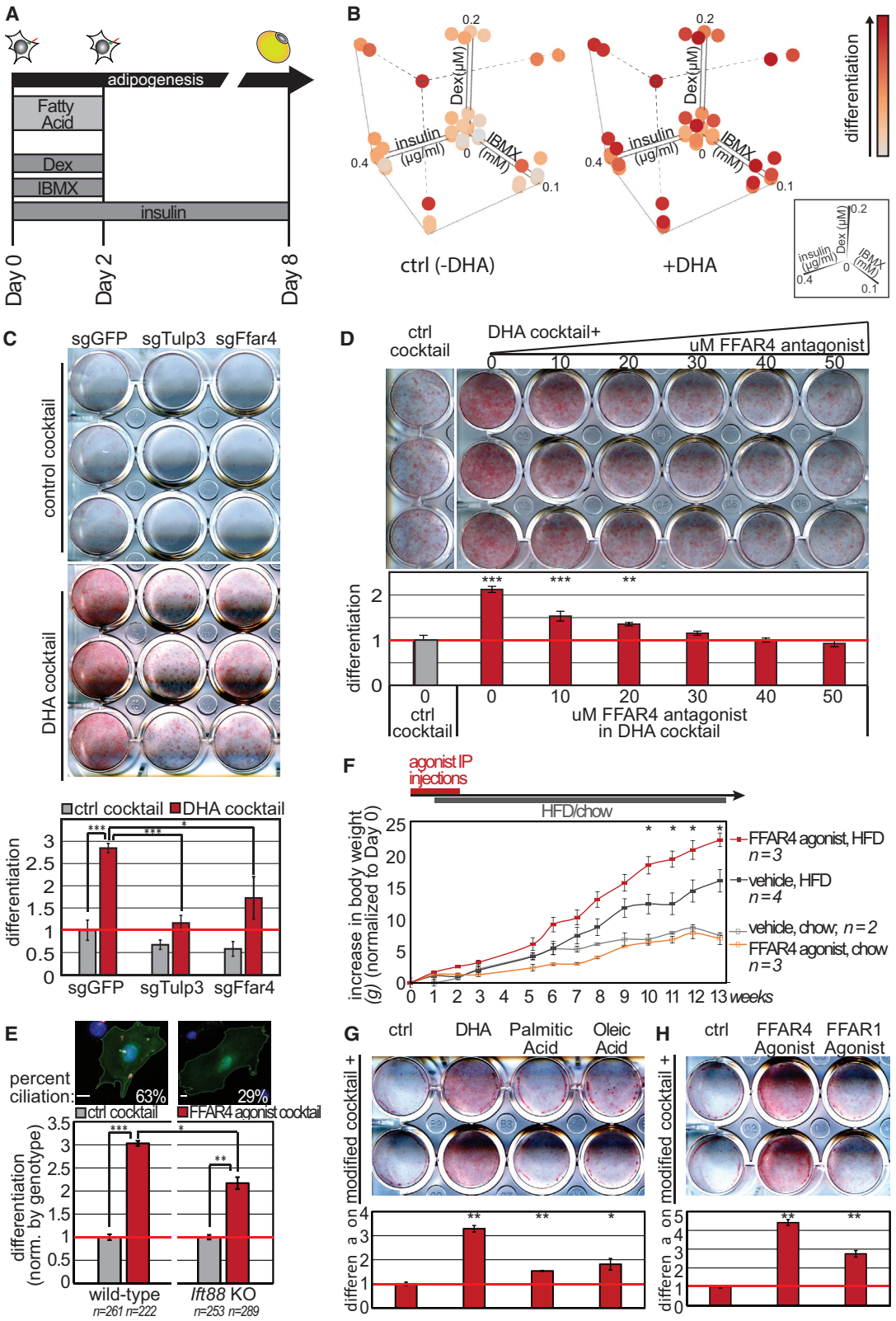

(legend on next page)

preadipocytes when FFAR4 expression is low. As the cilium is lost and FFAR4 expression increases during adipogenesis, the protein localizes to the plasma membrane, where it can regulate glucose uptake in mature adipocytes (Figure S4I) (Oh et al., 2010). Thus, FFAR4 is a newly identified ciliary GPCR that can localize to primary cilia of preadipocytes both *in vitro* and *in vivo* in a TULP3-dependent manner.

Activation of Ciliary FFAR4 Drives Early Steps in Adipogenesis

Given the requirement for TULP3 in adipogenesis, we hypothesized that FFAR4 in preadipocyte cilia promotes early adipogenesis, whereas FFAR4 on the plasma membrane of mature adipocytes has a distinct role. FFAR4 is activated by long-chain free fatty acids and, specifically, ω-3 fatty acids (Hirasawa et al., 2005; Oh et al., 2010). We therefore assessed how supplementing DM with the ω-3 fatty acid DHA affects adipogenesis (Figure 5A). Previous studies on the effect of free fatty acids on adipogenesis have yielded conflicting results, likely due to differences in DM composition and timing of free fatty acid supplementation (Kim et al., 2006; Madsen et al., 2005; Song et al., 2016). Thus, we added DHA during the first two days of differentiation, when FFAR4 is exclusively ciliary, and titrated the individual DM components in the presence and absence of DHA to determine dosages with greatest DHA potentiation (henceforth referred to as DHA cocktail and control cocktail, respectively; Figure S5A). Consistent with the requirement for TULP3 in adipogenesis, DHA potentiates adipogenesis when individual DM components are reduced (Figure 5B).

Free fatty acids have previously been proposed to be ligands of PPARγ (Krey et al., 1997). To confirm that DHA functions as an extracellular signaling molecule to promote adipogenesis, rather than as a PPARγ agonist, we stimulated 3T3-L1 cells with the DHA cocktail in the presence of the PPARγ antagonist T0070907. This antagonist is a potent inhibitor of adipogenesis when present during the entire differentiation time course (days 0–6), consistent with PPARγ being required for adipogenesis. However, when the PPARγ antagonist was added concurrently with DHA (days 0–2), it did not inhibit adipogenesis (Figure S5B). DHA therefore does not promote adipogenesis by directly activating PPARγ.

Instead, DHA-enhanced adipogenesis is dependent on FFAR4 and ciliary FFAR4 localization, since DHA failed to enhance adipogenesis in 3T3-L1 cells lacking TULP3 or FFAR4 (Figures 5C and S3B). Similarly, addition of the FFAR4 antagonist AH-7614 (days 0–2) inhibited DHA-enhanced adipogenesis in a dose-dependent manner (Figure 5D). 3T3-L1 differentiation in the DHA cocktail was more sensitive to the FFAR4 antagonist when compared to the standard, historical DM (Figure S5C). Thus, DHA functions as an extracellular signaling molecule to promote adipogenesis. Moreover, FFAR4 agonist promoted adipogenesis of primary mouse preadipocytes, and FFAR4 antagonism inhibited adipogenesis of primary human preadipocytes, suggesting that FFAR4 is broadly required for adipogenesis (Figures S5D and S5E).

To further validate our *in vitro* findings, we isolated primary preadipocytes from *Ift88*$^{flox/flox}$ and wild-type males and induced loss of cilia by transducing with an adenovirus expressing both Cre recombinase and GFP. Cre removed cilia from primary *Ift88*$^{flox/flox}$ preadipocytes but not from primary wild-type preadipocytes (Figure 5E). Similarly, primary *Ift88*$^{flox/flox}$ preadipocytes expressing GFP only possessed cilia (Figure S5F). Notably, loss of cilia impaired the ability of FFAR4 agonist to promote adipogenesis of primary preadipocytes (Figures 5E and S5F). Thus, DHA, a physiological ligand for FFAR4, promotes adipogenesis of 3T3-L1 preadipocytes as well as primary murine preadipocytes via primary cilia.

We investigated whether FFAR4 activation also promotes adipogenesis *in vivo*. Mice were injected daily with FFAR4 agonist for 2 weeks, and they were switched to an HFD starting the second week for a total of 3 months. We sequentially administered the agonist followed by an HFD, since our *in vitro* data showed that FFAR4 activation in the early phase of adipogenesis is sufficient to promote adipogenesis. Consistent with our *ex vivo* data, pretreatment with FFAR4 agonist causes a dramatic and synergistic increase in body weight when combined with an HFD (Figure 5F).

We next considered whether different types of fatty acids promote adipogenesis. Intriguingly, only the FFAR4 ligand DHA, but not saturated or mono-unsaturated palmitic or oleic acid, significantly and robustly potentiated adipogenesis (Figure 5G). Thus, DHA is selectively able to drive FFAR4-mediated adipogenesis, in contrast to saturated or mono-unsaturated fatty acids, which may instead drive hypertrophy of mature adipocytes. Of note, the ω-3 fatty acid DHA can activate FFAR1 in addition to FFAR4 (Ichimura et al., 2014). Only FFAR4 localizes to cilia (data not shown). Using the specific pharmacological agonists TUG891 (FFAR4) and TUG424 (FFAR1), we found that activating FFAR4 (but not FFAR1) during the first 2 days of differentiation promoted 3T3-L1 adipogenesis (Figure 5H). Thus, we establish

Figure 5. FFAR4 Activation Promotes Adipogenesis

(A) Schematic of 3T3-L1 differentiation experiment in the presence of free fatty acids.

(B) 3D mesh plot of differentiation using different amounts of insulin, Dex, and IBMX in the presence or absence of 100 μM DHA during the first 2 days of differentiation. Data plotted are normalized absorbance post-isopropanol extraction of oil red O (images in Figure S4A).

(C and D) DHA cocktail enhances differentiation of 3T3-L1 cells, and this is attenuated by (C) loss of TULP3 or FFAR4 protein or (D) addition of FFAR4 antagonist (AH7614) in a dose-dependent manner.

(E) FFAR4 activation promotes adipogenesis of primary mouse preadipocytes (Lin^-, $CD34^+$, $SCA1^+$, $CD29^+$) from wild-type, but not *Ift88*$^{flox/flox}$, post-transduction with Cre recombinase and GFP. n, number of GFP+ cells counted. Scale bar, 10 μm.

(F) Daily FFAR4 agonist intraperitoneal injection followed by HFD increases diet-induced obesity. All data are mean ± SEM; n, number of mice. p values calculated using standard t test comparing FFAR4 agonist HFD versus vehicle HFD.

(G) Supplementing DHA, but not palmitic acid or oleic acid, enhances adipogenesis.

(H) Addition of FFAR4, but not FFAR1, agonist enhances adipogenesis. Bar graphs are normalized mean ± SD. *$p < 0.05$; **$p < 0.01$; ***$p < 0.001$.

See also Figure S5.

that DHA and FFAR4 are a physiologically relevant ligand-receptor pair that is organized by preadipocyte cilia to promote adipogenesis.

DHA and FFAR4 Promote Adipogenesis by Raising Ciliary cAMP Levels

We sought to identify the molecular mechanism by which DHA promotes adipogenesis. First, we confirmed, using fluorescence microscopy, that DHA cocktail promoted adipogenesis by activating more preadipocytes to differentiate. The number of lipid-containing adipocytes increased as assessed by the lipophilic green fluorescent BODIPY dye both in an endpoint assay and kinetically during the differentiation time course (Figures 6A and 6B). Moreover, adipogenic genes were induced and pre-adipocyte genes were downregulated in response to DHA cocktail (Figure S6A). Thus, DHA promotes more preadipocytes to differentiate.

We investigated at which point in the adipogenic program DHA acts. Activation of quiescent preadipocytes *in vitro* and *in vivo* causes rapid cell cycle re-entry prior to induction of PPARγ. In 3T3-L1 cells, mitoses occur during the first 2 days of differentiation. To determine whether DHA promotes cell cycle re-entry in 3T3-L1 cells, we assessed EdU incorporation 40 h after addition of DHA or control cocktail and found that DHA promoted re-entry into the cell cycle (Figures 6C and S6B). Thus, DHA is mitogenic in this context and initiates the adipogenic program. Importantly, the mitogenic function of DHA is dependent on ciliary FFAR4 localization, since 3T3-L1 cells lacking TULP3 fail to undergo mitosis in response to DHA cocktail. In contrast, cell cycle re-entry in response to the historical DM is independent of TULP3 (Figures S6B and S6C). These data are consistent with our previous results showing that high levels of glucocorticoids uncouple initiation of adipogenesis from sensing of extracellular cues (Figure 3B) and strongly argue that the DHA cocktail described here is more physiologically relevant to adipogenesis.

In particular, we considered that free fatty acids, unlike pharmacological components in DM such as Dex and IBMX, may be *in vivo* regulators of adipogenesis. We therefore hypothesized that one or more components in DM (insulin, Dex, and IBMX) mimic the effect of DHA to initiate adipogenesis. To test this hypothesis, we serially omitted each component in the presence or absence of FFAR4 agonist. We note that some insulin and IGF1 are present in the serum, although at amounts insufficient to trigger robust adipogenesis. FFAR4 activation can replace IBMX, a phosphodiesterase inhibitor that raises cellular levels of the second messenger cAMP, and can also partially substitute for insulin (Figures 6D and S6D). We therefore hypothesized that FFAR4 activation promotes adipogenesis by signaling via cAMP specifically in the primary cilium.

To test our hypothesis, we transduced 3T3-L1 preadipocytes with a ciliary-targeted cAMP sensor (cilia cADDIS) optimized for live cell imaging (Moore et al., 2016). Increased ciliary cAMP caused decreased ciliary green fluorescence signal of the cADDIS sensor. We quantified dynamic changes in cAMP levels as the ratio of green fluorescence to red fluorescence reference (generated by a constitutively ciliary-localized mCherry fusion protein). Strikingly, addition of FFAR4 agonist TUG-891 rapidly increased ciliary cAMP levels in confluent 3T3-L1 preadipocytes (Figures 6E and 6F). This increase occurred within seconds of treatment and was dependent on ciliary localization of FFAR4, as loss of TULP3 prevented ciliary cAMP signaling in 3T3-L1 cells (Figure S6E).

We investigated which cAMP second messenger system mediates the cAMP signal. cAMP can activate at least two downstream pathways, protein kinase A (PKA) and exchange factor directly activated by cAMP (EPAC). To determine which of these pathways is activated by ciliary FFAR4, we titrated increasing amounts of established PKA or EPAC inhibitors onto 3T3-L1 cells differentiating in DHA cocktail. Inhibition of EPAC, but not PKA, prevented DHA-enhanced adipogenesis (Figure 6G). Specifically, EPAC inhibitor ESI-09 attenuated adipogenesis induced by DHA cocktail at levels consistent with its reported IC_{50} (~5 μM), whereas high-level (125 μM) PKA inhibitor Rp-cAMPs (IC_{50} ~ 5 μM) did not. Thus, DHA initiates the adipogenic program through activation of localized ciliary cAMP and EPAC, resulting in cell cycle re-entry. Moreover, DHA can replace IBMX as a differentiation factor to induce adipogenesis *in vitro*.

DHA and FFAR4-Induced Adipogenesis Require CTCF, a Regulator of Chromatin Architecture

Having identified ciliary cAMP and EPAC as mediators of DHA cocktail-induced adipogenesis, we examined how FFAR4 affects the adipogenic transcriptional program. Adipogenic transcriptional regulators collectively activate two adipogenic master transcription factors, PPARγ and CEBPα. DHA cocktail induces PPARγ and CEBPα (Figures 7A, 7B, and S7A). To understand the kinetics of PPARγ activation, we generated a reporter 3T3-L1 cell line, appending an open reading frame encoding a self-cleaving peptide T2A and green fluorescent protein to the 3′ end of the endogenous PPARγ locus, such that induction of PPARγ can be monitored by assessing green fluorescence intensity over time. PPARγ was induced after 48 h of DHA cocktail treatment, and this was FFAR4 dependent (Figure S7B).

We assessed the expression and activation of known early adipogenic transcription factors and regulators. DHA cocktail induced many known adipogenic factors, including the CEBPβ transcription factor and phosphorylation of AKT, ERK, and CREB (Figures S7C and S7D). However, while these adipogenic mediators were required for DHA cocktail-induced adipogenesis (Figure S7E), control cocktail (DHA) induced equivalent phosphorylation of AKT, ERK, and CREB (Figures S7C and S7D), arguing that these previously described adipogenic regulators are not specifically induced by DHA.

We therefore performed unbiased next-generation sequencing to identify gene expression changes specifically induced by DHA. Specifically, we compared gene expression of confluent, undifferentiated 3T3-L1 cells to 3T3-L1 cells treated with historical DM, DHA cocktail, or control cocktail for 24 h (Table S2). There was a dramatic shift in gene expression for all three induction conditions, even at this early time point (Figure 7C). Since both DM and DHA cocktail, but not control cocktail, promote robust adipogenesis, these data argue that most of the gene expression changes observed are not important for adipogenesis. Specifically, the ~1,300 gene changes induced by DM only and the ~100 genes controlled by the DHA cocktail only may not be relevant to adipogenesis, focusing us on the

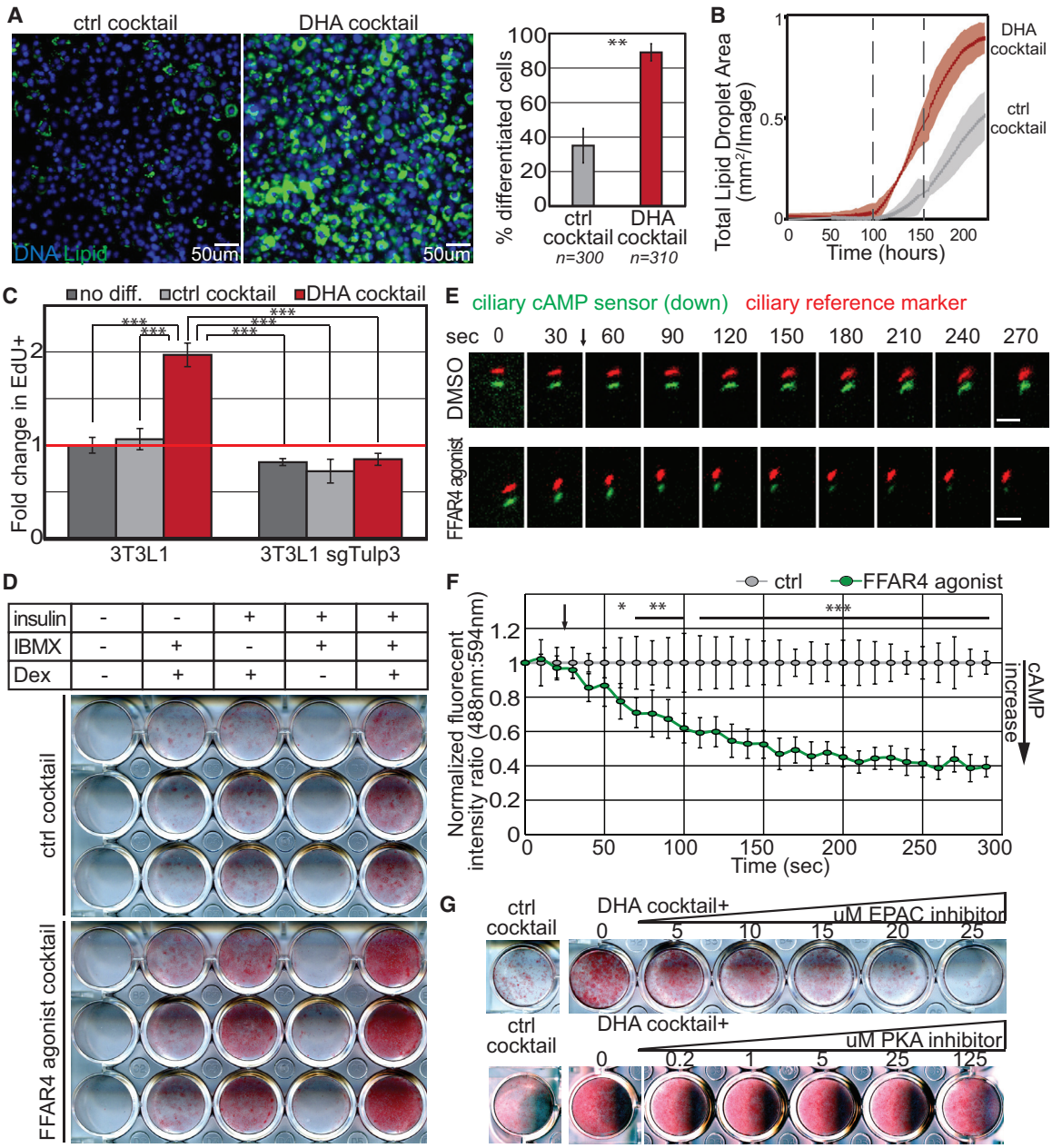

Figure 6. FFAR4 Regulates Initiation of Adipogenesis via cAMP

(A and B) DHA cocktail initiates adipogenesis in 3T3-L1 cells (A) after 6 days of differentiation and (B) as assessed by the increase in lipid droplets (BODIPY) over time. Data are average of 3 wells ± SD; shaded area is 95% confidence interval. Dotted line denotes media change. n, number of cells counted. Scale bar, 50 μm.

(C) DHA cocktail results in cell cycle re-entry, and this requires TULP3 protein. Bar graphs show normalized average from 3 experiments ± SD.

(D) 3T3-L1 cells were exposed to individual components of the modified cocktail ± FFAR4 agonist for 48 h. FFAR4 activation partially replaces IBMX.

(E and F) FFAR4 activation elevates ciliary cAMP levels. 3T3-L1 cells were transduced with a ciliary cAMP sensor (green) and reference marker (red). Addition of FFAR4 agonist (denoted by arrow) results in decreased ciliary green fluorescence intensity, indicating that ciliary cAMP levels increase.

(E) Representative images showing cAMP sensor (green) and cilia (red) offset. Scale bar, 5 μm.

(F) Background subtracted ratio of fluorescence intensities are normalized to DMSO control and 0 s time point. n = 6 for FFAR4 agonist, and n = 4 for DMSO control ± SD, where n is the average of all cilia measured per well.

(G) 3T3-L1 cells were differentiated with DHA cocktail in the presence of an inhibitor against EPAC (ESI-09) or PKA (Rp-cAMPS) for the first 2 days. Lipid accumulation was assessed on day 4. Inhibition of EPAC, but not PKA, attenuates DHA enhanced adipogenesis in a dose-dependent manner. *p < 0.05; **p < 0.01; ***p < 0.001.

See also Figure S6.

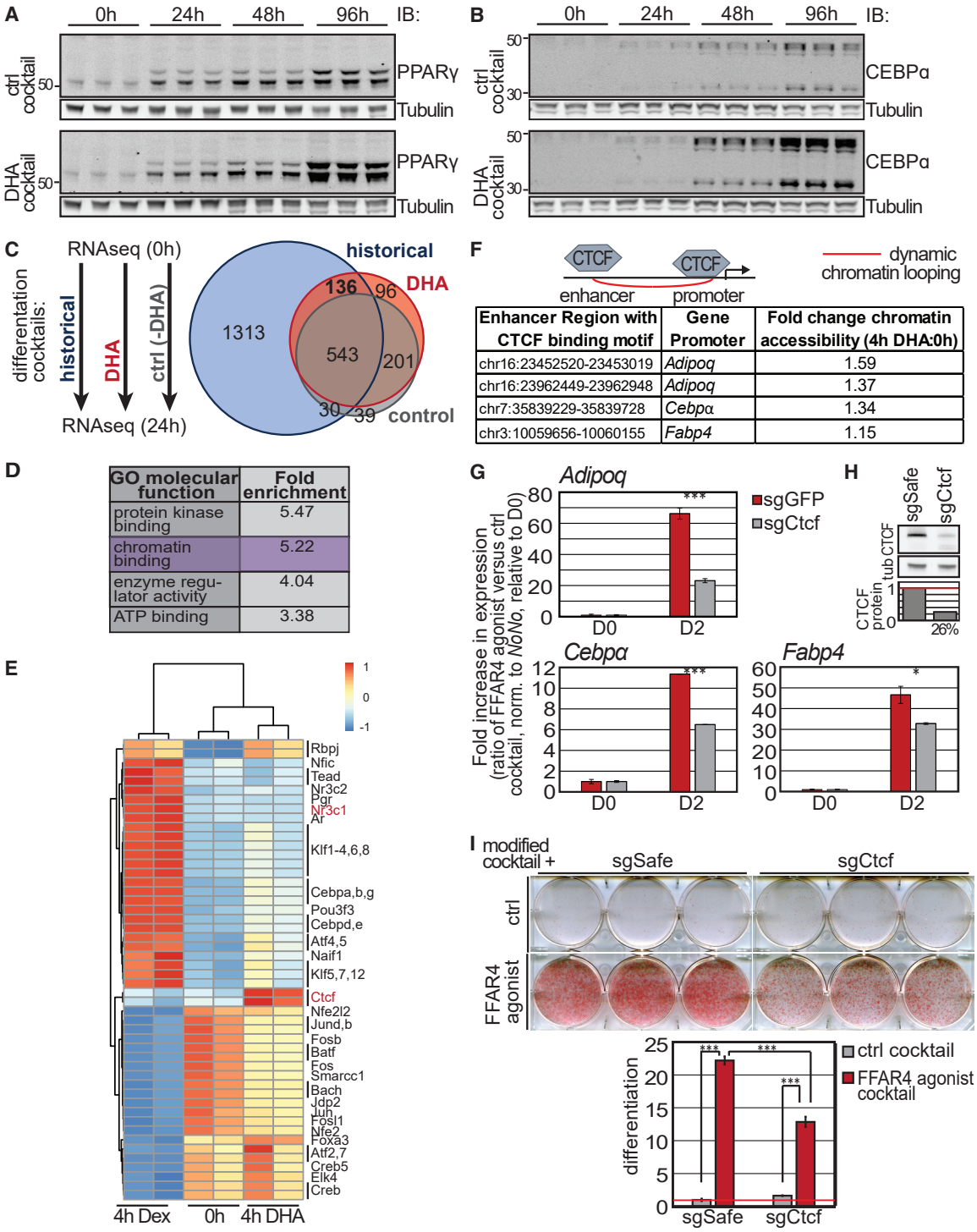

Figure 7. FFAR4 Activates PPARγ and CEBPα via CTCF-Dependent Chromatin Remodeling

(A and B) Addition of DHA cocktail to 3T3-L1 cells increased (A) PPARγ and (B) CEBPα protein levels. 3 independent samples are shown per time point.

(C and D) Schematic of next-generation RNA-sequencing experiment (left). 3T3-L1 cells were treated for 24 h with ctrl cocktail, DHA cocktail, or historical DM. (C) Venn diagram of all significantly altered genes ($q < 0.05$) with greater than 2-fold up- or downregulation compared to 0 h (right). Data describe 3 independent experiments.

(D) Gene ontology enrichment analysis of all genes significantly upregulated by more than 2 fold in response to both DHA cocktail and historical DM.

(legend continued on next page)

136 genes that were induced by both. The smaller number of genes affected by the DHA cocktail provides additional evidence that this formulation may be more physiologically relevant to the initiation of adipogenesis.

To further explore the genes upregulated by both DM and DHA cocktail, we analyzed gene ontology, which suggested that chromatin binding may be regulated (Figure 7D). We assessed how DHA treatment affects chromatin accessibility by performing an assay for transposase-accessible chromatin sequencing (ATACseq) at different differentiation time points followed by transcription factor motif analysis (Table S3). We specifically compared chromatin accessibility of confluent, undifferentiated 3T3-L1 cells with 3T3-L1 cells treated with DHA only for 4 h, since this is the earliest time point at which we observe consistent changes in chromatin accessibility (data not shown), and we wanted to interrogate the direct effects of DHA and not secondary effects due to initiation of the adipogenic transcriptional program. As a general control for the ATACseq method, we also assessed chromatin accessibility of 3T3-L1 cells treated with Dex alone for 4 h, a well-established glucocorticoid receptor agonist that mediates DNA binding of its receptor. Transcription factor motif analysis confirmed that Dex treatment caused a dramatic increase in chromatin opening at glucocorticoid receptor (Nr3c1) binding sites as well at sites for adipogenic transcription factors such as CEBP proteins and KLF proteins (Figure 7E). Intriguingly, DHA treatment increased chromatin access at CTCF binding motifs (Figure 7E). CTCF is a regulator of transcription and chromatin architecture. Thus, these data suggest that DHA promotes adipogenesis by inducing CTCF-mediated chromatin remodeling to activate the adipogenic transcriptional program.

Previous studies have shown dynamic chromatin remodeling of promoter-enhancer interactions during 3T3-L1 differentiation including at CTCF binding sites and that these interactions correlate with adipogenic gene expression (Dubois-Chevalier et al., 2014; Siersbaek et al., 2017). We hypothesized that DHA induces adipogenesis by promoting formation of chromatin loops between enhancers and promoters of adipogenic genes in a CTCF-dependent manner. To test this hypothesis, we identified which CTCF motif-containing regions were opened in response to DHA as well as the proximal promoters (Table S4). CTCF was recruited to regulatory regions for *Adipoq*, *Cebp*α, and *Fabp4* (Figure 7F).

To further test our hypothesis that CTCF mediates DHA-enhanced adipogenesis, we generated 3T3-L1 cells lacking CTCF (Figures 7H and S7I). Loss of CTCF did not affect cell proliferation (Figure S7F). We induced adipogenesis of control and *Ctcf* knockout cells with DHA cocktail. Expression of *Adipoq*, *Cebp*α, and *Fabp4* were induced, and this was partially dependent on CTCF (Figure 7G). Moreover, loss of CTCF significantly attenuated DHA-mediated adipogenesis (Figure 7I) but had no effect on adipogenesis induced by the historical DM (Figure S7G). We confirmed that CTCF is required for DHA-enhanced adipogenesis in multiple independent 3T3-L1 cell lines lacking CTCF (Figures S7H and S7I). Thus, DHA may promote adipogenesis by inducing formation of chromatin loops between enhancers and the promoters of adipogenic genes via CTCF.

DISCUSSION

By focusing on the primary cilium of preadipocytes, we have identified a strong candidate for a physiologically relevant ligand-receptor pair that activates early events in adipogenesis. We found that primary cilia identify preadipocytes *in vivo*. Genetic ablation of cilia in preadipocytes blocks adipogenesis *in vivo* and strongly reduces fat mass. The underlying molecular mechanism requires signaling by the ω-3 fatty acid receptor FFAR4/GPR120 at preadipocyte cilia. DHA activates ciliary FFAR4, resulting in a rapid increase in ciliary cAMP levels. Ciliary cAMP in turn promotes adipogenesis by activating the EPAC effector protein, a guanine-nucleotide exchange factor. DHA induces chromatin remodeling through CTCF, inducing adipogenic genes and adipogenesis. Several key conclusions emerge.

ω-3 Fatty Acids Promote Adipogenesis through FFAR4

This current study establishes a cell autonomous signaling function for FFAR4 in initiating adipogenesis in preadipocytes. Specifically, *in vivo*, *ex vivo*, and *in vitro* loss of preadipocyte ciliation impairs adipogenesis, while activation of ciliary FFAR4 signaling dramatically promotes adipogenesis. We do not understand why we did not observe systemic hallmarks of lipodystrophy despite the dramatic failure to expand WAT tissue in $PA^{no\ cilia}$ mice, and we propose that the residual amount of WAT in $PA^{no\ cilia}$ mice (~5 g) was sufficient to buffer the extra expended energy within the experimental time frame. We further postulate that removing preadipocyte cilia prior to 3 weeks of age, extending the physiological analysis beyond 20 weeks of age, or feeding mice an HFD could reveal systemic metabolic consequences of preadipocyte ciliation loss.

Previous studies have described the metabolic role of FFAR4 in promoting glucose uptake in adipocyte and in mediating the systemic anti-diabetic effects of ω-3 fatty acids, including DHA (Ichimura et al., 2012; Oh et al., 2010; Oh et al., 2014; Suckow et al., 2014). Taken together, our data suggest that the anti-diabetic effects of DHA and FFAR4 are mediated in part by shifting WAT expansion toward hyperplasia rather than adipocyte

(E) Chromatin accessibility as assessed by ATAC-seq shows enrichment of CTCF binding motifs in open chromatin after 4 h of DHA-only treatment.
(F) Known enhancer-adipogenic gene promoter loops that contain a CTCF binding motif and are opened by DHA. Fold change describes average increase in accessibility from 2 independent experiments.
(G) Loss of CTCF attenuates expression of adipogenic genes in response to FFAR4 activation. Bar graph is average of three independent experiments ± SD. Expression normalized to housekeeping gene *NoNo*.
(H) Immunoblot showing depletion of CTCF protein in 3T3-L1 cells.
(I) CTCF is required for 3T3-L1 adipogenesis induced by FFAR4 agonist cocktail. Bar graphs are normalized mean ± SD. *$p < 0.05$; ***$p < 0.001$.
See also Figure S7.

hypertrophy or deposition of fat in other tissues, including liver. These data provide a possible understanding of the anti-diabetic effects of dietary DHA supplementation: DHA increases the generation of more adipocytes with lower fat content per adipocyte.

A Mitogenic Role for ω-3 Fatty Acids: Nutritive Fluxes Trigger Cell-Cycle Entry and Stem Cell Expansion

In preadipocytes, cAMP is important for cell cycle re-entry and differentiation, reflected by the inclusion of IBMX in the historical DM. By replacing IBMX with DHA and establishing a direct and rapid link to cAMP elevation in the primary cilium, we link a physiological ligand to cAMP production in preadipocytes. This finding raises critical questions. What is the threshold for DHA signaling *in vivo*? Are there differential responses in different WAT depots? How do other adipogenic factors, such as insulin, affect DHA signaling?

Epigenetic Programs for Adipogenesis

The importance of transcription factors in controlling adipogenesis is well characterized (Rosen et al., 2000). The chromatin regulatory factors that cooperate with adipogenic transcription factors are less well identified. A recent study highlighted a dynamic rewiring of promoter-enhancer loops by 3T3-L1 preadipocytes within 4 h of initiation of adipogenesis (Siersbaek et al., 2017). We found that 4 h of Dex-only treatment opens chromatin and affects transcription factor binding, consistent with previous reports (Siersbæk et al., 2012). CTCF, a factor important for organizing chromatin loops, mediates DHA-dependent adipogenesis by promoting expression of the adipogenic genes such as *Adipoq*, *Cebpα*, and *Fabp4*. Further investigation may determine how adipogenic signals, including DHA, control CTCF function and chromatin looping.

The Primary Cilium as a Sensor of Multiple Growth Factors and Nutrients

There is growing appreciation for the primary cilium as a sensory organelle. We show that preadipocytes *in vitro* and *in vivo* are ciliated and that ciliated perivascular cells account for almost 30% of all perivascular cells. It remains to be elucidated how uniform or heterogeneous this population may be with regard to stemness and adipogenic potential, and further studies to define stem cell and signaling populations will be important. It would be particularly interesting to examine ciliation in preadipocyte subpopulations within fat tissue, as recently revealed through the use of single-cell sequencing (Burl et al., 2018; Hepler et al., 2018; Merrick et al., 2019; Schwalie et al., 2018).

Mice lacking ciliated preadipocytes fail to expand WAT *in vivo*, highlighting the importance of cilia to mesenchymal progenitor cell function and raising the possibility that defects in mesenchymal progenitor cells may contribute to human ciliopathies. The ciliary DHA/FFAR4 signaling pathway provides a molecular hypothesis about how ciliary dysfunction in ciliopathies may contribute to metabolic dysfunction. A recent study also described that adipose-derived mesenchymal stem cells (ASCs) from WAT of obese individuals display shorter, signaling-defective cilia compared to ASCs isolated from lean WAT, suggesting that obesity may also impact ciliary signaling (Ritter et al., 2018). Future investigations are required to determine whether defective ciliary FFAR4 signaling leads to metabolic dysfunction.

The primary cilium likely senses multiple pro- and anti-adipogenic signals, but the interplay of different ciliary signaling pathways within a single cilium is unclear. Conceivably, the primary cilium integrates multiple signals, organizing outputs to secondary messengers, including cAMP and calcium. 3T3-L1 primary cilia, in addition to FFAR4, display IGF-1 receptor (Zhu et al., 2009). Our data show that DHA can partially substitute for insulin, raising the possibility of crosstalk between DHA and insulin signaling at the cilium.

FFAR4 Signaling in Ciliated Preadipocytes versus Mature, Unciliated Adipocytes

FFAR4 expression increases dramatically during adipogenesis, and the receptor is highly expressed in mature unciliated adipocytes. As the primary cilium is a cylinder with an approximate diameter of 200–300 nm and a median length of 3–5 μm, an average adipocyte with a diameter of 100 μm would need to express almost 10,000 times more FFAR4 receptors to achieve the same receptor density as is achieved by ciliary FFAR4 in preadipocytes. We propose that concentrating FFAR4 in the cilium sensitizes its responses to enable the initiation of adipogenesis in perivascular preadipocytes and that DHA and FFAR4-mediated activation of CTCF may provide a robust mechanism for sustaining expression of high levels of FFAR4 in mature adipocytes.

Differentiated unciliated cells may therefore repurpose formerly ciliary receptors, and, in the same tissue, ciliated and unciliated cells may use the same receptor to activate distinct effector pathways at different subcellular locales to coordinate the overall tissue response to a ligand. DHA can promote tissue expansion by initiating adipogenesis of preadipocytes and promoting hypertrophy of adipocytes (Oh et al., 2010). Confining FFAR4 to the primary cilium in preadipocytes, versus the plasma membrane in mature adipocyte, may selectively activate distinct effector pathways; our data suggest that ciliary FFAR4 in preadipocytes couples to $G_{\alpha s}$, while FFAR4 in the plasma membrane of mature adipocytes has previously been shown to couple to $G_{\alpha q}$ (Oh et al., 2010). This differential coupling may allow for distinct responses to DHA for cells of different states within the same tissue.

Saturated versus Unsaturated Fatty Acids: How to Make Healthy Fat

The ability to both deposit and mobilize fatty acids in response to nutritive cues is critical for fat to remain metabolically healthy (Ghaben and Scherer, 2019). Defective fatty acid transport can lead to adipose tissue inflammation, fibrosis, and diabetes. We have found that an ω-3 fatty acid, DHA, stimulates expansion of preadipocytes, but saturated and mono-unsaturated fatty acids do not. Accordingly, the proportion of ω-3 and saturated fatty acids, and the ability to sense this ratio, may determine the balance between hyperplastic and hypertrophic adipose tissue expansion. Consistently, ω-3 fatty acid supplementation results in improved insulin sensitivity and decreased adipose tissue inflammation in humans and mice (Gao et al., 2017; Oh et al., 2010; Spencer et al., 2013).

STAR★METHODS

Detailed methods are provided in the online version of this paper and include the following:

- KEY RESOURCES TABLE
- LEAD CONTACT AND MATERIALS AVAILABILITY
- EXPERIMENTAL MODEL AND SUBJECT DETAILS
  - *In vivo* animal studies
  - Cell line models
- METHOD DETAILS
  - Plasmids
  - Cell Line generation
  - Immunofluorescence staining
  - Immunohistochemistry
  - Antibody generation
  - Whole mount white adipose staining
  - Epi-fluorescence and confocal imaging
  - *In vitro* Adipogenesis
  - Isolation of primary preadipocytes
  - Sample preparation and immunoblot
  - Glucose and serum analysis
  - Oil red O staining for lipid visualization and quantification
  - Live Cell Imaging Analysis for adipogenesis and proliferation
  - Echo-MRI and CLAMS
  - Quantitative Real time PCR
  - EdU incorporation for cell cycle analysis
  - Live Cell Ciliary cAMP assay
  - PPARγ reporter cell line generation
  - Next generation RNA sequencing and analysis
  - ATACseq and TF motif enrichment analysis
- QUANTIFICATION AND STATISTICAL ANALYSIS
- DATA AND CODE AVAILABILITY

SUPPLEMENTAL INFORMATION

Supplemental Information can be found online at https://doi.org/10.1016/j.cell.2019.11.005.

ACKNOWLEDGMENTS

P.K.J. was supported by NIH grants 5R01GM114276, 5U01CA199216, and 5UL1TR00108502 and the Stanford Department of Research and Baxter Laboratory. J.F.R. was supported by NIH grants AR054396, DK106404, and GM095941. D.K. was supported by departmental startup funds. K.I.H. is a Layton Family Fellow of the Damon Runyon Cancer Research Foundation (DRG-2210-14). C.T.J. is supported by an NIH training grant (TG2-01159). A.M. is supported by the Swedish Research Council (grant 2015-06403). J.F.R. and W.J.G. are Chan Zuckerberg Biohub investigators. We thank N. Mooney for animal husbandry support. We thank the UCSF Diabetes Research Center, especially Chris Paillart, for help with the CLAMS and EchoMRI studies. We thank Kevin Corbit and Jennifer Tran for assistance with serum analysis.

AUTHOR CONTRIBUTIONS

Conceptualization, K.I.H., D.K., and P.K.J.; Methodology, K.I.H., C.T.J., and D.K.; Software, A.M. and J.D.; Investigation, K.I.H., C.T.J., A.M., D.K., A.M.N., and S.L.R.; Resources, W.G.G., J.F.R., and P.K.J.; Writing – Original Draft, K.I.H.; Writing – Review & Editing, K.I.H., D.K., J.F.R., and P.K.J.; Supervision, K.I.H., D.K., J.F.R., and P.K.J.; Funding Acquisition, J.F.R. and P.K.J.

DECLARATION OF INTERESTS

The authors declare no competing interests.

Received: August 26, 2018
Revised: September 23, 2019
Accepted: October 31, 2019
Published: November 21, 2019

REFERENCES

Anders, S., Pyl, P.T., and Huber, W. (2015). HTSeq–a Python framework to work with high-throughput sequencing data. Bioinformatics *31*, 166–169. Published online September 25, 2014.

Arner, P., Andersson, D.P., Thörne, A., Wirén, M., Hoffstedt, J., Näslund, E., Thorell, A., and Rydén, M. (2013). Variations in the size of the major omentum are primarily determined by fat cell number. J. Clin. Endocrinol. Metab. *98*, E897–E901.

Ashburner, M., Ball, C.A., Blake, J.A., Botstein, D., Butler, H., Cherry, J.M., Davis, A.P., Dolinski, K., Dwight, S.S., Eppig, J.T., et al.; The Gene Ontology Consortium (2000). Gene ontology: tool for the unification of biology. Nat. Genet. *25*, 25–29.

Bangs, F.K., Schrode, N., Hadjantonakis, A.K., and Anderson, K.V. (2015). Lineage specificity of primary cilia in the mouse embryo. Nat. Cell Biol. *17*, 113–122.

Berry, R., and Rodeheffer, M.S. (2013). Characterization of the adipocyte cellular lineage in vivo. Nat. Cell Biol. *15*, 302–308.

Brinkman, E.K., Chen, T., Amendola, M., and van Steensel, B. (2014). Easy quantitative assessment of genome editing by sequence trace decomposition. Nucleic Acids Res. *42*, e168.

Buenrostro, J.D., Wu, B., Chang, H.Y., and Greenleaf, W.J. (2015). ATAC-seq: a method for assaying chromatin accessibility genome-wide. Curr. Protoc. Mol. Biol. *109*, 21–29.

Burl, R.B., Ramseyer, V.D., Rondini, E.A., Pique-Regi, R., Lee, Y.H., and Granneman, J.G. (2018). Deconstructing adipogenesis induced by beta3-adrenergic receptor activation with single-cell expression profiling. Cell Metab. *28*, 300–309.e304.

Corces, M.R., Trevino, A.E., Hamilton, E.G., Greenside, P.G., Sinnott-Armstrong, N.A., Vesuna, S., Satpathy, A.T., Rubin, A.J., Montine, K.S., Wu, B., et al. (2017). An improved ATAC-seq protocol reduces background and enables interrogation of frozen tissues. Nat. Methods *14*, 959–962.

Crenn, P., Morin, M.C., Joly, F., Penven, S., Thuillier, F., and Messing, B. (2004). Net digestive absorption and adaptive hyperphagia in adult short bowel patients. Gut *53*, 1279–1286.

Davenport, J.R., Watts, A.J., Roper, V.C., Croyle, M.J., van Groen, T., Wyss, J.M., Nagy, T.R., Kesterson, R.A., and Yoder, B.K. (2007). Disruption of intraflagellar transport in adult mice leads to obesity and slow-onset cystic kidney disease. Curr. Biol. *17*, 1586–1594.

Deren, M.E., Yang, X., Guan, Y., and Chen, Q. (2016). Biological and chemical removal of primary cilia affects mechanical activation of chondrogenesis markers in chondroprogenitors and hypertrophic chondrocytes. Int. J. Mol. Sci. *17*, 188.

Dobin, A., Davis, C.A., Schlesinger, F., Drenkow, J., Zaleski, C., Jha, S., Batut, P., Chaisson, M., and Gingeras, T.R. (2013). STAR: ultrafast universal RNA-seq aligner. Bioinformatics *29*, 15–21.

Dubois-Chevalier, J., Oger, F., Dehondt, H., Firmin, F.F., Gheeraert, C., Staels, B., Lefebvre, P., and Eeckhoute, J. (2014). A dynamic CTCF chromatin binding landscape promotes DNA hydroxymethylation and transcriptional induction of adipocyte differentiation. Nucleic Acids Res. *42*, 10943–10959.

Forcioli-Conti, N., Lacas-Gervais, S., Dani, C., and Peraldi, P. (2015). The primary cilium undergoes dynamic size modifications during adipocyte

differentiation of human adipose stem cells. Biochem. Biophys. Res. Commun. *458*, 117–122.

Ford, M.J., Yeyati, P.L., Mali, G.R., Keighren, M.A., Waddell, S.H., Mjoseng, H.K., Douglas, A.T., Hall, E.A., Sakaue-Sawano, A., Miyawaki, A., et al. (2018). A cell/cilia cycle biosensor for single-cell kinetics reveals persistence of cilia after G1/S transition is a general property in cells and mice. Dev. Cell *47*, 509–523 e505.

Fu, W., Asp, P., Canter, B., and Dynlacht, B.D. (2014). Primary cilia control hedgehog signaling during muscle differentiation and are deregulated in rhabdomyosarcoma. Proc. Natl. Acad. Sci. USA *111*, 9151–9156.

Gao, H., Geng, T., Huang, T., and Zhao, Q. (2017). Fish oil supplementation and insulin sensitivity: a systematic review and meta-analysis. Lipids Health Dis. *16*, 131.

Ghaben, A.L., and Scherer, P.E. (2019). Adipogenesis and metabolic health. Nat. Rev. Mol. Cell Biol. *20*, 242–258.

Gotoh, C., Hong, Y.H., Iga, T., Hishikawa, D., Suzuki, Y., Song, S.H., Choi, K.C., Adachi, T., Hirasawa, A., Tsujimoto, G., et al. (2007). The regulation of adipogenesis through GPR120. Biochem. Biophys. Res. Commun. *354*, 591–597.

Guimaraes-Camboa, N., Cattaneo, P., Sun, Y., Moore-Morris, T., Gu, Y., Dalton, N.D., Rockenstein, E., Masliah, E., Peterson, K.L., Stallcup, W.B., et al. (2017). Pericytes of multiple organs do not behave as mesenchymal stem cells in vivo. Cell Stem Cell *20*, 345–359.e345.

Gupta, R.K., Mepani, R.J., Kleiner, S., Lo, J.C., Khandekar, M.J., Cohen, P., Frontini, A., Bhowmick, D.C., Ye, L., Cinti, S., and Spiegelman, B.M. (2012). Zfp423 expression identifies committed preadipocytes and localizes to adipose endothelial and perivascular cells. Cell Metab. *15*, 230–239.

Haczeyni, F., Bell-Anderson, K.S., and Farrell, G.C. (2018). Causes and mechanisms of adipocyte enlargement and adipose expansion. Obes. Rev. *19*, 406–420.

Haycraft, C.J., Zhang, Q., Song, B., Jackson, W.S., Detloff, P.J., Serra, R., and Yoder, B.K. (2007). Intraflagellar transport is essential for endochondral bone formation. Development *134*, 307–316.

Hepler, C., Vishvanath, L., and Gupta, R.K. (2017). Sorting out adipocyte precursors and their role in physiology and disease. Genes Dev. *31*, 127–140.

Hepler, C., Shan, B., Zhang, Q., Henry, G.H., Shao, M., Vishvanath, L., Ghaben, A.L., Mobley, A.B., Strand, D., Hon, G.C., and Gupta, R.K. (2018). Identification of functionally distinct fibro-inflammatory and adipogenic stromal subpopulations in visceral adipose tissue of adult mice. eLife *7*, e39636.

Hildebrandt, F., Benzing, T., and Katsanis, N. (2011). Ciliopathies. N. Engl. J. Med. *364*, 1533–1543.

Hilgendorf, K.I., Johnson, C.T., and Jackson, P.K. (2016). The primary cilium as a cellular receiver: organizing ciliary GPCR signaling. Curr. Opin. Cell Biol. *39*, 84–92.

Hirasawa, A., Tsumaya, K., Awaji, T., Katsuma, S., Adachi, T., Yamada, M., Sugimoto, Y., Miyazaki, S., and Tsujimoto, G. (2005). Free fatty acids regulate gut incretin glucagon-like peptide-1 secretion through GPR120. Nat. Med. *11*, 90–94.

Huang-Doran, I., and Semple, R.K. (2010). Knockdown of the Alström syndrome-associated gene Alms1 in 3T3-L1 preadipocytes impairs adipogenesis but has no effect on cell-autonomous insulin action. Int. J. Obes. *34*, 1554–1558.

Hwang, S.H., Somatilaka, B.N., Badgandi, H., Palicharla, V.R., Walker, R., Shelton, J.M., Qian, F., and Mukhopadhyay, S. (2019). Tulp3 regulates renal cystogenesis by trafficking of cystoproteins to cilia. Curr. Biol. *29*, 790–802.e795.

Ichimura, A., Hirasawa, A., Poulain-Godefroy, O., Bonnefond, A., Hara, T., Yengo, L., Kimura, I., Leloire, A., Liu, N., Iida, K., et al. (2012). Dysfunction of lipid sensor GPR120 leads to obesity in both mouse and human. Nature *483*, 350–354.

Ichimura, A., Hasegawa, S., Kasubuchi, M., and Kimura, I. (2014). Free fatty acid receptors as therapeutic targets for the treatment of diabetes. Front. Pharmacol. *5*, 236.

Jaafar Marican, N.H., Cruz-Migoni, S.B., and Borycki, A.G. (2016). Asymmetric distribution of primary cilia allocates satellite cells for self-renewal. Stem Cell Reports *6*, 798–805.

Jeffery, E., Church, C.D., Holtrup, B., Colman, L., and Rodeheffer, M.S. (2015). Rapid depot-specific activation of adipocyte precursor cells at the onset of obesity. Nat. Cell Biol. *17*, 376–385.

Jeffery, E., Wing, A., Holtrup, B., Sebo, Z., Kaplan, J.L., Saavedra-Peña, R., Church, C.D., Colman, L., Berry, R., and Rodeheffer, M.S. (2016). The adipose tissue microenvironment regulates depot-specific adipogenesis in obesity. Cell Metab. *24*, 142–150.

Jiang, Y., Berry, D.C., Tang, W., and Graff, J.M. (2014). Independent stem cell lineages regulate adipose organogenesis and adipose homeostasis. Cell Rep. *9*, 1007–1022.

Jones, T.R., Kang, I.H., Wheeler, D.B., Lindquist, R.A., Papallo, A., Sabatini, D.M., Golland, P., and Carpenter, A.E. (2008). CellProfiler Analyst: data exploration and analysis software for complex image-based screens. BMC Bioinformatics *9*, 482.

Kang, S.H., Fukaya, M., Yang, J.K., Rothstein, J.D., and Bergles, D.E. (2010). NG2+ CNS glial progenitors remain committed to the oligodendrocyte lineage in postnatal life and following neurodegeneration. Neuron *68*, 668–681.

Karastergiou, K., and Fried, S.K. (2017). Cellular mechanisms driving sex differences in adipose tissue biology and body shape in humans and mouse models. Adv. Exp. Med. Biol. *1043*, 29–51.

Kelly, D.J., and Jacobs, C.R. (2010). The role of mechanical signals in regulating chondrogenesis and osteogenesis of mesenchymal stem cells. Birth Defects Res. C Embryo Today *90*, 75–85.

Kim, S., and Dynlacht, B.D. (2013). Assembling a primary cilium. Curr. Opin. Cell Biol. *25*, 506–511.

Kim, H.K., Della-Fera, M., Lin, J., and Baile, C.A. (2006). Docosahexaenoic acid inhibits adipocyte differentiation and induces apoptosis in 3T3-L1 preadipocytes. J. Nutr. *136*, 2965–2969.

Kolde, R. (2015). Pheatmap: pretty heatmaps. R package, version 108.

Kopinke, D., Roberson, E.C., and Reiter, J.F. (2017). Ciliary hedgehog signaling restricts injury-induced adipogenesis. Cell *170*, 340–351.e312.

Krey, G., Braissant, O., L'Horset, F., Kalkhoven, E., Perroud, M., Parker, M.G., and Wahli, W. (1997). Fatty acids, eicosanoids, and hypolipidemic agents identified as ligands of peroxisome proliferator-activated receptors by coactivator-dependent receptor ligand assay. Mol. Endocrinol. *11*, 779–791.

Langmead, B., and Salzberg, S.L. (2012). Fast gapped-read alignment with Bowtie 2. Nat. Methods *9*, 357–359.

Loktev, A.V., and Jackson, P.K. (2013). Neuropeptide Y family receptors traffic via the Bardet-Biedl syndrome pathway to signal in neuronal primary cilia. Cell Rep. *5*, 1316–1329.

Love, M.I., Huber, W., and Anders, S. (2014). Moderated estimation of fold change and dispersion for RNA-seq data with DESeq2. Genome Biol. *15*, 550.

Lyu, R., and Zhou, J. (2017). The multifaceted roles of primary cilia in the regulation of stem cell properties and functions. J. Cell. Physiol. *232*, 935–938.

Madsen, L., Petersen, R.K., and Kristiansen, K. (2005). Regulation of adipocyte differentiation and function by polyunsaturated fatty acids. Biochim. Biophys. Acta *1740*, 266–286.

Marion, V., Stoetzel, C., Schlicht, D., Messaddeq, N., Koch, M., Flori, E., Danse, J.M., Mandel, J.L., and Dollfus, H. (2009). Transient ciliogenesis involving Bardet-Biedl syndrome proteins is a fundamental characteristic of adipogenic differentiation. Proc. Natl. Acad. Sci. USA *106*, 1820–1825.

Marion, V., Mockel, A., De Melo, C., Obringer, C., Claussmann, A., Simon, A., Messaddeq, N., Durand, M., Dupuis, L., Loeffler, J.P., et al. (2012). BBS-induced ciliary defect enhances adipogenesis, causing paradoxical higher-insulin sensitivity, glucose usage, and decreased inflammatory response. Cell Metab. *16*, 363–377.

Martin, M. (2011). Cutadapt removes adapter sequences from high-throughput sequencing eads. EMBnetjournal *17*, 10–12.

Merrick, D., Sakers, A., Irgebay, Z., Okada, C., Calvert, C., Morley, M.P., Percec, I., and Seale, P. (2019). Identification of a mesenchymal progenitor cell hierarchy in adipose tissue. Science *364*, eaav2501.

Moore, B.S., Stepanchick, A.N., Tewson, P.H., Hartle, C.M., Zhang, J., Quinn, A.M., Hughes, T.E., and Mirshahi, T. (2016). Cilia have high cAMP levels that are inhibited by Sonic Hedgehog-regulated calcium dynamics. Proc. Natl. Acad. Sci. USA *113*, 13069–13074.

Mukhopadhyay, S., Wen, X., Chih, B., Nelson, C.D., Lane, W.S., Scales, S.J., and Jackson, P.K. (2010). TULP3 bridges the IFT-A complex and membrane phosphoinositides to promote trafficking of G protein-coupled receptors into primary cilia. Genes Dev. *24*, 2180–2193.

Nachury, M.V., Loktev, A.V., Zhang, Q., Westlake, C.J., Peränen, J., Merdes, A., Slusarski, D.C., Scheller, R.H., Bazan, J.F., Sheffield, V.C., and Jackson, P.K. (2007). A core complex of BBS proteins cooperates with the GTPase Rab8 to promote ciliary membrane biogenesis. Cell *129*, 1201–1213.

O'Rourke, M., Cullen, C.L., Auderset, L., Pitman, K.A., Achatz, D., Gasperini, R., and Young, K.M. (2016). Evaluating tissue-specific recombination in a Pdgfrα-CreERT2 transgenic mouse line. PLoS ONE *11*, e0162858.

Oh, D.Y., Talukdar, S., Bae, E.J., Imamura, T., Morinaga, H., Fan, W., Li, P., Lu, W.J., Watkins, S.M., and Olefsky, J.M. (2010). GPR120 is an omega-3 fatty acid receptor mediating potent anti-inflammatory and insulin-sensitizing effects. Cell *142*, 687–698.

Oh, D.Y., Walenta, E., Akiyama, T.E., Lagakos, W.S., Lackey, D., Pessentheiner, A.R., Sasik, R., Hah, N., Chi, T.J., Cox, J.M., et al. (2014). A Gpr120-selective agonist improves insulin resistance and chronic inflammation in obese mice. Nat. Med. *20*, 942–947.

Palmer, A.K., and Kirkland, J.L. (2016). Aging and adipose tissue: potential interventions for diabetes and regenerative medicine. Exp. Gerontol. *86*, 97–105.

Qiu, N., Cao, L., David, V., Quarles, L.D., and Xiao, Z. (2010). Kif3a deficiency reverses the skeletal abnormalities in Pkd1 deficient mice by restoring the balance between osteogenesis and adipogenesis. PLoS ONE *5*, e15240.

Ritter, A., Friemel, A., Kreis, N.N., Hoock, S.C., Roth, S., Kielland-Kaisen, U., Brüggmann, D., Solbach, C., Louwen, F., and Yuan, J. (2018). Primary cilia are dysfunctional in obese adipose-derived mesenchymal stem cells. Stem Cell Reports *10*, 583–599.

Rodeheffer, M.S., Birsoy, K., and Friedman, J.M. (2008). Identification of white adipocyte progenitor cells in vivo. Cell *135*, 240–249.

Rosen, E.D., and Spiegelman, B.M. (2014). What we talk about when we talk about fat. Cell *156*, 20–44.

Rosen, E.D., Walkey, C.J., Puigserver, P., and Spiegelman, B.M. (2000). Transcriptional regulation of adipogenesis. Genes Dev. *14*, 1293–1307.

Sakaguchi, M., Fujisaka, S., Cai, W., Winnay, J.N., Konishi, M., O'Neill, B.T., Li, M., García-Martín, R., Takahashi, H., Hu, J., et al. (2017). Adipocyte dynamics and reversible metabolic syndrome in mice with an inducible adipocyte-specific deletion of the insulin receptor. Cell Metab. *25*, 448–462.

Schep, A.N., Wu, B., Buenrostro, J.D., and Greenleaf, W.J. (2017). chromVAR: inferring transcription-factor-associated accessibility from single-cell epigenomic data. Nat. Methods *14*, 975–978.

Schmittgen, T., and Livak, K. (2008). Analyzing real-time PCR data by the comparative C_T method. Nature Protocols *3* (6), 1101–1108.

Schwalie, P.C., Dong, H., Zachara, M., Russeil, J., Alpern, D., Akchiche, N., Caprara, C., Sun, W., Schlaudraff, K.U., Soldati, G., et al. (2018). A stromal cell population that inhibits adipogenesis in mammalian fat depots. Nature *559*, 103–108.

Siersbæk, R., Nielsen, R., and Mandrup, S. (2012). Transcriptional networks and chromatin remodeling controlling adipogenesis. Trends Endocrinol. Metab. *23*, 56–64.

Siersbaek, R., Madsen, J.G.S., Javierre, B.M., Nielsen, R., Bagge, E.K., Cairns, J., Wingett, S.W., Traynor, S., Spivakov, M., Fraser, P., et al. (2017). Dynamic rewiring of promoter-anchored chromatin loops during adipocyte differentiation. Mol. Cell *66*, 420–435.e425.

Siljee, J.E., Wang, Y., Bernard, A.A., Ersoy, B.A., Zhang, S., Marley, A., Von Zastrow, M., Reiter, J.F., and Vaisse, C. (2018). Subcellular localization of MC4R with ADCY3 at neuronal primary cilia underlies a common pathway for genetic predisposition to obesity. Nat. Genet. *50*, 180–185.

Song, T., Zhou, Y., Peng, J., Tao, Y.X., Yang, Y., Xu, T., Peng, J., Ren, J., Xiang, Q., and Wei, H. (2016). GPR120 promotes adipogenesis through intracellular calcium and extracellular signal-regulated kinase 1/2 signal pathway. Mol. Cell. Endocrinol. *434*, 1–13.

Spencer, M., Finlin, B.S., Unal, R., Zhu, B., Morris, A.J., Shipp, L.R., Lee, J., Walton, R.G., Adu, A., Erfani, R., et al. (2013). Omega-3 fatty acids reduce adipose tissue macrophages in human subjects with insulin resistance. Diabetes *62*, 1709–1717.

Srinivas, S., Watanabe, T., Lin, C.S., William, C.M., Tanabe, Y., Jessell, T.M., and Costantini, F. (2001). Cre reporter strains produced by targeted insertion of EYFP and ECFP into the ROSA26 locus. BMC Dev. Biol. *1*, 4.

Stewart, S.A., Dykxhoorn, D.M., Palliser, D., Mizuno, H., Yu, E.Y., An, D.S., Sabatini, D.M., Chen, I.S., Hahn, W.C., Sharp, P.A., et al. (2003). Lentivirus-delivered stable gene silencing by RNAi in primary cells. RNA *9*, 493–501.

Suckow, A.T., Polidori, D., Yan, W., Chon, S., Ma, J.Y., Leonard, J., and Briscoe, C.P. (2014). Alteration of the glucagon axis in GPR120 (FFAR4) knockout mice: a role for GPR120 in glucagon secretion. J. Biol. Chem. *289*, 15751–15763.

Tang, Q.Q., Otto, T.C., and Lane, M.D. (2003). Mitotic clonal expansion: a synchronous process required for adipogenesis. Proc. Natl. Acad. Sci. USA *100*, 44–49.

Tang, W., Zeve, D., Suh, J.M., Bosnakovski, D., Kyba, M., Hammer, R.E., Tallquist, M.D., and Graff, J.M. (2008). White fat progenitor cells reside in the adipose vasculature. Science *322*, 583–586.

Tummala, P., Arnsdorf, E.J., and Jacobs, C.R. (2010). The role of primary cilia in mesenchymal stem cell differentiation: a pivotal switch in guiding lineage commitment. Cell. Mol. Bioeng. *3*, 207–212.

Vishvanath, L., MacPherson, K.A., Hepler, C., Wang, Q.A., Shao, M., Spurgin, S.B., Wang, M.Y., Kusminski, C.M., Morley, T.S., and Gupta, R.K. (2016). Pdgfrβ+ mural preadipocytes contribute to adipocyte hyperplasia induced by high-fat-diet feeding and prolonged cold exposure in adult mice. Cell Metab. *23*, 350–359.

Wang, Q.A., Tao, C., Gupta, R.K., and Scherer, P.E. (2013). Tracking adipogenesis during white adipose tissue development, expansion and regeneration. Nat. Med. *19*, 1338–1344.

Waters, A.M., and Beales, P.L. (2011). Ciliopathies: an expanding disease spectrum. Pediatr. Nephrol. *26*, 1039–1056.

Weisberg, S.P., McCann, D., Desai, M., Rosenbaum, M., Leibel, R.L., and Ferrante, A.W., Jr. (2003). Obesity is associated with macrophage accumulation in adipose tissue. J. Clin. Invest. *112*, 1796–1808.

Xiao, Z.S., and Quarles, L.D. (2010). Role of the polycytin-primary cilia complex in bone development and mechanosensing. Ann. N Y Acad. Sci. *1192*, 410–421.

Yuan, X., and Yang, S. (2016). Primary cilia and intraflagellar transport proteins in bone and cartilage. J. Dent. Res. *95*, 1341–1349.

Zhu, D., Shi, S., Wang, H., and Liao, K. (2009). Growth arrest induces primary-cilium formation and sensitizes IGF-1-receptor signaling during differentiation induction of 3T3-L1 preadipocytes. J. Cell Sci. *122*, 2760–2768.

STAR★METHODS

KEY RESOURCES TABLE

REAGENT or RESOURCE	SOURCE	IDENTIFIER
Antibodies		
BrdU	Cell Signaling	Cat# 5292
FFAR4	this work	n/a
FFAR4 (sc)	santa cruz	Cat# sc-390752
PPARG	Cell signaling	Cat# 2435
Tubulin	Sigma	Cat# 9026
CEBPA	Cell signaling	Cat# 8178
CTCF	Cell signaling	Cat# 2899
ERK	Cell signaling	Cat# 9107
pERK	Cell signaling	Cat# 9101
AKT	Cell signaling	Cat# 9272
pAKT	Cell signaling	Cat# 9271
CREB	Cell signaling	Cat# 9104
pCREB	Cell signaling	Cat# 9198
GFP	Invitrogen	Cat# A10262
CD45 PE-Cy7	eBioscience	Cat# 25-0451-81
CD31 PE-Cy7	eBioscience	Cat# 25-0311-81
Ter119 PE-Cy7	eBioscience	Cat# 25-5921-81
CD34 Alexa Fluor 700	eBioscience	Cat# 56-0341-82
CD29 APC	eBioscience	Cat# 17-0291-80
TULP3	Mukhopadhyay et al., 2010	N/A
CEP170	Thermo	Cat# 41-3200
ARL13B	NeuroMab	Cat# 73-287
Sca1 Pacific Blue	Biolegend	Cat# 108120
Pericentrin	Covance	Cat# PRB-432C
GFP	Avis Lab	Cat# 1020
PDGFRA	R&D Systems	Cat# AF1062
ARL13B	Proteintech	Cat# 17711-1-AP
Acetylated tubulin	Sigma	Cat# T7451
FGFR1OP	Novus	Cat# H00011116-M01
MAC-2	cederlane	Cat# cl8942ap
KI-67	Millipore	Cat# AB9260
CD31	BD	Cat# 553370
Bacterial and Virus Strains		
One Shot® Stbl3™ Chemically Competent *E. coli*	Invitrogen	Cat# C7373-03
One Shot® ccdB Survival™ 2 T1R Competent Cells	Invitrogen	Cat# A10460
MAX Efficiency DH10B Competent Cells	Invitrogen	Cat# 18297-010
Cre recombinant Adenovirus	Vector BioLabs	Cat# 1045N
Cre GFP Recombinase Adenovirus	Vector BioLabs	Cat# 1700
eGFP Adenovirus	Vector BioLabs	Cat# 1060
Chemicals, Peptides, and Recombinant Proteins		
IBMX	Sigma	Cat# I7018
DHA	Sigma	Cat# D2534

(*Continued on next page*)

Continued

REAGENT or RESOURCE	SOURCE	IDENTIFIER
Palmitic Acid	Sigma	Cat# D0500
Oleic Acid	Sigma	Cat# O01383
TUG891	Tocris	Cat# 4601
TUG424	Tocris	Cat# 3785
DharmaFECT 1 Transfection Reagent	Dharmacon	Cat# T-2001-03
Fugene6	Promega	Cat# PR-E2691
DAPI	Bio Trend	Cat# 40043
BODIPY 493/503	Thermo	Cat# D-3922
LIPIDTOX	Thermo	Cat# H34475
CTRL DIET	ResearchDiets	Cat# D12450J
60% high fat diet	ResearchDiets	Cat# D12492
Ratiometric Cilia-Targete cADDis cAMP	Molecular Montana	Cat# D0211G
ESI 09	Tocris	Cat# 4773
MK2260	Santa Cruz	Cat# sc-364537
U0126	Tocris	Cat# 1144
BrdU	Abcam	Cat# ab142567
Sodium Tetraborate decahydrate	Sigma	Cat# B9876
AH7614	R&D Systems	Cat# 5256/10
Tamoxifen	Sigma	Cat# T-5648
Breeder Chow	Lab Diet	Cat# 5058
Insulin	Sigma	Cat# I-5500
Bovine Calf serum	Sigma	Cat# 12133C
Pen/Strep	Thermo	Cat# 15140163
GlutaMax	life	Cat# 35050-079
DMEM	Thermo	Cat# 11995065
Preadipocyte Growth Medium	PromoCell	Cat# C-27410
Preadipocyte Differentiation Medium	PromoCell	Cat# C-27436
Adipocyte Nutrition Medium	PromoCell	Cat# C-27438
Paraformaldehyde	AlfaAesar	Cat# 433689M
Normal Donkey Serum	Jackson ImmunoResearch	Cat# 017-000-121
NP40	Sigma	Cat# 11332473001
Dexamethazone	Sigma	Cat# D4902
polybrene	Millipore	Cat# TR-1003-G
saponin	Sigma	Cat# 7900
Fluoromount-G	SouthernBiotech	Cat# 0100-01
FFAR4 peptide: Cys-PILYNMSLFRNEWRK	Yenzym	n/a
Mounting media	Dako	Cat# C056330-2
Dabco	Sigma	Cat# D27802-25G
Collagenase	Sigma	Cat# C6885
DNase	Worthington	Cat# LS006344
P-188	Sigma	Cat# P5556
Medium 199	Sigma	Cat# M4530
Histopaq-1077	Sigma	Cat# 10771
anti-CD45 microbeads	Miltenyi	Cat# 130-052-301
anti-TER119 microbeads	Miltenyi	Cat# 130-049-901
Oil Red O	Sigma	Cat# 00625
M-MLV Reverse Transcriptase	Invitrogen	Cat# 28025-013

(*Continued on next page*)

Continued

REAGENT or RESOURCE	SOURCE	IDENTIFIER
TaqMan Gene Expression Master Mix	Applied Biosystems	Cat# 4369016
Digitonin	Promega	Cat# G9441
PowerUP SYBR green	Invitrogen	Cat# A25741
Critical Commercial Assays		
insulin ELISA	ALPCO	Cat# 80-INSMSU-E01
Leptin ELISA	ALPCO	Cat# 22-LEPMS-E01
Free Fatty Acid ELISA	Wako	Cat# NEFA-HR2
Click-iT EdU Imaging Kit	Thermo	Cat# C10340
Deposited Data		
RNaseq	this work	GEO: GSE118471
PCHi-C	Siersbaek et al., 2017	GEO: GSE95533
ATACseq	this work	GEO: GSE118470
Experimental Models: Cell Lines		
3T3-L1 sgGFP	this work	N/A
3T3-L1 sgTulp3	this work	N/A
3T3-L1 sgGFP LAPN-TULP3	this work	N/A
3T3-L1 sgTulp3 LAPN-TULP3	this work	N/A
3T3-L1 LAPC FFAR4	this work	N/A
3T3-L1 LAPC SMO	this work	N/A
3T3-L1 sgSafe	this work	N/A
3T3-L1 sgCtcf_1	this work	N/A
3T3-L1 sgCtcf_2	this work	N/A
3T3-L1 sgCtcf_3	this work	N/A
3T3-L1	Bernard Allan	N/A
Primary human preadipocytes	PromoCell	Cat# C-12730
Experimental Models: Organisms/Strains		
Mouse: C57BL/6J	Jackson Laboratories	Cat# 000664
Mouse: B6.129P2-*Ift88*^{tm1Bky}/J)	Jackson Laboratory; Haycraft et al., 2007	Cat# 022409
Mouse: CD1 mice	Charles River	Cat# 021
Mouse: *Gt(ROSA)26Sor*$^{tm1(EYFP)Cos}$	Jackson Laboratory	Cat# 006148
Mouse: *Tg(Pdgfrα-cre/ERT)467Dbe*	Jackson Laboratory	Cat# 018280
Mouse: Tg(CAG-Arl13b/mCherry)1Kvand Tg(CAG-EGFP/CETN2)3-4Jgg/KvandJ	Jackson Laboratories; Bangs et al., 2015	Cat# 027967
Mouse: Ffar4$^{tm1(KOMP)Vlcg}$	KOMP Repository	Cat# VG15078
Oligonucleotides		
siPparg	Dharmacon	Cat# L-040712-00
siTulp3_1	Integrated DNA Technologies	Cat# MMC.RNAI.N011657.12.1
siTulp3_2	Integrated DNA Technologies	Cat# MMC.RNAI.N011657.12.2
siTulp3_3	Integrated DNA Technologies	Cat# MMC.RNAI.N011657.12.3
siCtrl	Integrated DNA Technologies; Dharmacon	51-01-14-03
DNA primer sequences, see Table S5	Integrated DNA Technologies, ElimBio	N/A
TaqMan probes, see Table S5	Life Technologies	N/A
Recombinant DNA		
pCMV-dR8.2 dvpr	Stewart et al., 2003	Addgene plasmid #8455
pCMV-VSV-G	Stewart et al., 2003	Addgene plasmid #8454
pENTR TULP3	Mukhopadhyay et al., 2010	N/A
pBabe LAPN-TULP3	this work	N/A

(*Continued on next page*)

Continued

REAGENT or RESOURCE	SOURCE	IDENTIFIER
pBabe LAPC-SMO	this work	N/A
pDONR221 SMO	Harvard Plasmid	HsCD00042333
pBabe LAPC-FFAR4	this work	N/A
pENTR223 FFAR4/GPR120	Harvard Plasmid	HsCD00370484
p306 sgGFP	this work	N/A
p306 sgFfar4	this work	N/A
p306 sgTulp3	this work	N/A
p306 sgSafe	this work	N/A
p306 sgCtcf_1	this work	N/A
p306 sgCtcf_2	this work	N/A
p306 sgCtcf_3	this work	N/A
p293 Cas9-BFP	Michael Bassik	N/A
pMCB306	Michael Bassik	N/A
Software and Algorithms		
SlideBook	3i (Intelligent Imaging Innovations)	https://www.intelligent-imaging.com/slidebook
TIDE analysis	Brinkman et al., 2019	https://tide.deskgen.com/
Plotly Image visualization	Plotly Technologies	https://plot.ly/
Graphpad Prism	Graphpad Software	https://www.graphpad.com/scientific-software/prism/
Geneious	Biomatters Limited	www.geneious.com
Kallisto	Pachter Lab	https://pachterlab.github.io/kallisto/
Sleuth	Pachter Lab	https://pachterlab.github.io/sleuth/about
Star	Dobin et al., 2013	https://github.com/alexdobin/STAR
Cutdiff	Trapnell Lab	http://cole-trapnell-lab.github.io/cufflinks/cuffdiff/
Htseq	Anders et al., 2015	https://htseq.readthedocs.io/en/release_0.10.0/overview.html
DESeq2	Love et al., 2014	http://bioconductor.org/packages/devel/bioc/vignettes/DESeq2/inst/doc/DESeq2.html
Bowtie2	Langmead and Salzberg, 2012	http://bowtie-bio.sourceforge.net/bowtie2/index.shtml
Samtools	GitHub	http://samtools.sourceforge.net/
chromVAR	Schep et al., 2017	https://bioconductor.org/packages/release/bioc/html/chromVAR.html
Bcl2fastq	Illumina	N/A
Cutadapt	Martin, 2011	N/A
Picard	Broad Institute	http://broadinstitute.github.io/picard
Pheatmap	Kolde, 2015	https://cran.r-project.org/web/packages/pheatmap/index.html
GO Enrichment analysis	Ashburner et al., 2000	http://geneontology.org/
LI-COR Image studio	LI-COR Biosciences	https://www.licor.com/
IncuCyte Zoom	Essen BioScience	https://www.essenbioscience.com/en/
Cell Profiler	Jones et al., 2008	www.cellprofiler.org
Photoshop CS5	Adobe	www.adobe.com
Canvas X	Canvas GFX Inc	https://www.canvasgfx.com/
CLAMS Examination Tool	Columbus Instruments	www.colinst.com
ImageJ	NIH	https://imagej.nih.gov/ij/

LEAD CONTACT AND MATERIALS AVAILABILITY

Further information and requests for resources and reagents should be directed to and will be fulfilled by the Lead Contact, Peter Jackson (pjackson@stanford.edu). All unique/stable reagents generated in this study are available from the Lead Contact with a completed Materials Transfer Agreement.

EXPERIMENTAL MODEL AND SUBJECT DETAILS

In vivo animal studies

Gt(ROSA)26Sor$^{tm1(EYFP)Cos}$ and *Pdgfrα*-CreERT mice (Tg(Pdgfrα-cre/ERT)467Dbe) have been described previously (Kang et al., 2010; Srinivas et al., 2001). *Ffar4* knockout mice in a C56BL/6 background were generated by *in vitro* fertilization using sperm from Ffar4$^{tm1(KOMP)Vlcg}$ obtained from KOMP. Cilia-Glow mice (Tg$^{(CAG-Arl13b/mCherry)1Kv}$ and Tg$^{(CAG-EGFP/CETN2)3-4Jgg/KvandJ)}$) were purchased from Jackson Laboratory (027967). Ift88$^{flox/flox}$ mice (B6.129P2-*Ift88*^{tm1Bky}/J$^{)}$) were purchased from Jackson Laboratory (022409). C57BL/6J mice were purchased from Jackson Laboratory (000664).

All mice were maintained under specific pathogen-free conditions at the Stanford and UCSF animal care facility. Mice were cared for and all experiments were approved by the Administrative Panel on Laboratory Care and the Institutional Animal Care and Use Committee (IACUC) of at Stanford University and UCSF. Animals were housed in groups of 5 adults per cage. Male mice between 6-8 weeks of age were used for isolation of murine primary preadipocytes and whole mount WAT imaging. Unless otherwise stated, mice were kept on normal chow diet. For the high fat diet experiments, male littermates between the ages of 6-8 were split and put on 60% HFD or the matched control diet (ResearchDiets D12492, D12450J). To measure *in vivo* activation of preadipocytes in response to HFD, mice were given BrdU (Abcam) in the drinking water at 0.8mg/mL for the entire duration of the HFD experiment (2 weeks), with fresh BrdU in the water provided every 2-3 days. To assess effects of TUG-891 on body weight, 9-week-old male C57BL/6J mice (JAX) were randomized to receive an intraperitoneal injection with either TUG-891 (35 mg/kg) or 10% dimethyl sulfoxide (DMSO) vehicle dissolved in corn oil once daily for 2 weeks. Starting the second week, mice were split and put on 60% HFD or the matched control diet (ResearchDiets D12492, D12450J) for 3 months. To assess the importance of preadipocyte ciliation, Tamoxifen (Sigma T-5648), dissolved in corn oil, was administered to *Pdgfrα*-CreERT *Ift88* conditional mice by oral gavage (200-250 mg/kg) on two consecutive days at 3 or 6 weeks of age and sex as indicated. In addition, all control mice regardless of gender or genotype also received tamoxifen. At day of tamoxifen treatment, mice were put on breeder chow (Lab Diet #5058). *Pdgfrα*-CreERT *Ift88* conditional mice were maintained by crossing to CD1 mice (Charles River).

Cell line models

3T3-L1 cells were cultured in DMEM medium containing 10% Bovine Calf Serum, 1% Pen/Strep, and 1% GlutaMAX and switched to DMEM containing 10% FBS, 1% Pen/Strep, and 1% GlutaMAX during adipogenesis.

Human white preadipocytes were cultured in Preadipocyte Growth Medium, differentiated in Preadipocyte Differentiation Medium, and adipocytes were maintained in Adipocyte Nutrition Medium (PromoCell).

Murine primary preadipocytes were isolated from inguinal or epididymal white adipose tissue from wild-type, cilia-glow, *Ffar4* knockout, and Ift88$^{flox/flox}$ male mice using mouse protocols approved by the Institutional Animal Care and Use Committee (IACUC) at Stanford University. Primary preadipocytes were maintained and differentiated in DMEM medium containing 10% FBS, 1% Pen/Strep, and 1% GlutaMAX.

METHOD DETAILS

Plasmids

pMCB306 (lentiviral vector, loxP-mU6-sgRNAs-puro resistance-EGFP-loxP) and p293 Cas9-BFP were gifts from Prof. Michael Bassik (Stanford University). pCMV-VSV-G and pCMV-dR8.2 dvpr were gifts from Prof. Bob Weinberg (Addgene plasmid #8454 and #8455) (Stewart et al., 2003). Lentiviral vectors containing sgRNA were generated by ligating annealed sgRNA oligonucleotides into pMCB306 vector digested with BstXI and BlpI restriction enzymes.

pBabe LAPN and LAPC plasmids are retroviral gateway destination vectors containing N- and C-terminal LAP (eGFP-TEV cleavage site-S tag-Precision cleavage) tags as previously described (Mukhopadhyay et al., 2010). Expression constructs were generated by Gateway LR reactions between entry clones and destination vectors.

Cell Line generation

Retroviral vectors carrying the gene of interest were transfected into Phoenix Eco-Env cells using Fugene6 (Promega), and lentiviral vectors carrying the gene of interest were co-transfected with pCMV-VSV-G and pCMV-dR8.2 dvpr into 293T cells. Media was replaced after 24 h and virus was harvested 48 and 72 h post-transfection. Virus was filtered with a 0.45 μm OVDF filter (Millipore) and used to infect cell lines with 10 μg/mL polybrene (Millipore). Media was replaced after 24 h and cells were sorted for GFP positivity after 48-72 h post-infection.

To generate Crispr/Cas9 knockout cells, 3T3-L1 Cas9-BFP cells were infected with lentivirus containing the sgRNA of interest. Knockout efficiency was determined 10 days post-infection by TIDE analysis (Brinkman et al., 2014). Primers listed in Table S5.

3T3-L1 cells expressing Cas9-BFP were generated by infection of virus harvested from 293T cells transfected with p293 Cas9-BFP, pCMV-VSV-G and pCMV-dR8.2 dvpr. 3T3-L1 Cas9-BFP cells were sorted for BFP positivity.

For rescue experiments of 3T3-L1 sgRNA cells, the sgRNA was removed by adenoviral infection with recombinant Cre, followed by sorting for GFP negativity.

For knockdown experiments using siRNA, 3T3-L1 cells were plated and transfected with 25nM siRNA after 24 h using DharmaFECT Reagent 1. Media was changed after 24 h, and differentiation was initiated 48 h post-transfection.

Immunofluorescence staining

Cells were grown on 12mm round coverslips and fixed with 4% paraformaldehyde (433689M, AlfaAesar) in PBS at room temperature for 10min. Samples were blocked with 5% normal donkey serum (017-000-121, Jackson ImmunoResearch) in IF buffer (for FFAR4 staining: 3% BSA and 0.4% saponin in PBS; for all else: 3% BSA and 0.1% NP-40 in PBS) at room temperature for 30min. Samples were incubated with primary antibody in IF buffer at room temperature for 1 h, followed by 5 washes with IF buffer. Samples were incubated with fluorescent-labeled secondary antibody at room temperature for 30min, followed by a 5 min incubation with 4',6-diamidino-2-phenylindole (DAPI) in PBS at room temperature for 5min and 5 washes with IF buffer. Coverslips were mounted with Fluoromount-G (0100-01, SouthernBiotech) onto glass slides followed by image acquisition. Antibodies were used as follows: Pericentrin (Covance, PRB-432C, 1:500), Acetylated tubulin (Sigma, T7451, 1:2000), CEP170 (Thermo, 41-3200, 1:500), ARL13B (UC Davis/NIH NeuroMab Facility, 73-287, 1:1000), FFAR4 (Yenzym, 1:500), FFAR4 (Santa Cruz, sc-390752, 1:100), FGFR1OP (Novus, H00011116-M01, 1:1000), GFP (Invitrogen, 1:2000, A10262).

Immunohistochemistry

WAT tissue was fixed in Zink-buffered formalin overnight at RT, paraffin embedded and sectioned. Tissue sections were de-waxed and rehydrated before undergoing standard Haemotoxylin and Eosin (H&E) staining. To assess the area of individual adipocytes, H&E stained WAT sections were thresholded and adipocyte area quantified using Analyze Particle function in ImageJ.

Antibody generation

The rabbit polyclonal antibody against FFAR4 was generated by rabbit injections (Yenzym, Cys-PILYNMSLFRNEWRK) followed by affinity purification using standard protocols.

Whole mount white adipose staining

Mice were perfused with PBS followed by 4% PFA in PBS. White adipose tissue was removed and cut into narrow strips and further fixed in 4% PFA and 0.3% Triton-X in PBS for 15min at room temperature. WAT strips were washed 3 times for a total of 1 h in 0.3% Triton-X/PBS (PBST) at room temperature and blocked overnight at 4C in 3% normal donkey serum/PBST. WAT strips were incubated with primary antibody in PBST for at least 6 h at room temperature, followed by 3 30min washes in PBST at room temperature. WAT strips were incubated with fluorescent-labeled secondary antibody (1:500) in PBST overnight at 4C, followed by incubation with 2 μg/mL DAPI/PBST for 30min at room temperature and 2 more 30min washes in PBST at room temperature. WAT strips were cut into small pieces ($\sim$2mm^3) and mounted with Glycergel Mounting media (Dako, C056330-2) containing 0.02 g/mL 1,4-Diazabicyclo[2.2.2]octane onto glass slides into a chamber created by stacking 2 coverslips.

For BrdU staining, the protocol was amended as follows: Strips of WAT post-fixation with PFA and 3 washes in PBST were incubated in 1N HCl at 37 C for 30min. WAT strips were then washed 3 times in PBS and incubated in 0.1M borate buffer (pH 8.5) for 10min. WAT strips were washed 3 times for 10min each in PBST and then blocked overnight followed by staining as described above.

Antibodies were used as follows: CD31 (BD, 553370, 1:200), Pericentrin (Covance, PRB-432C, 1:500), Acetylated tubulin (Sigma, T7451, 1:1000), BrdU (Cell Signaling, 5292, 1:500), GFP (1:1000, Avis lab #1020), PDGFRα (1:2500, R&D Systems #AF1062), ARL13B (1:1000, Proteintech #17711-1-AP), LipidTox (1:250, Invitrogen, H34475).

Epi-fluorescence and confocal imaging

Images were acquired on an Everest deconvolution workstation (Intelligent Imaging Innovations) equipped with a Zeiss AxioImager Z1 microscope and a CoolSnapHQ cooled CCD camera (Roper Scientific) and a 40x NA1.3 Plan-Apochromat objective lens (420762-9800, Zeiss) was used.

Confocal images were acquired on a Marianas spinning disk confocal (SDC) microscopy (Intelligent Imaging Innovations).

For Figures 2 and S2, images were acquired using a Leica DMi8 microscope equipped with a DFC7000T color camera (bright field images) as well as the SPE confocal system (immunofluorescence).

In vitro Adipogenesis

3T3-L1 cells were grown to confluency in DMEM containing 10% Bovine Calf Serum, followed by another 2 days at confluency in DMEM containing 10% Bovine Calf Serum. Adipogenesis was then induced using DMEM containing 10% FBS and differentiation cocktail consisting of insulin, dexamethasone, IBMX and/or DHA. 1x DM is 1 μg/mL insulin, 1 μM Dex, 0.5mM IBMX. DHA cocktail

is 0.4 μg/mL insulin, 0.02mM IBMX, 0.1 μM Dex, 100 μM DHA. FFAR4 agonist cocktail is 0.4 μg/mL insulin, 0.02mM IBMX, 0.1 μM Dex, 100 μM TUG891. Ctrl cocktail is 0.4 μg/mL insulin, 0.02mM IBMX, 0.1 μM Dex, EtOH/DMSO. Where noted, palmitic acid was added at 100 μM, oleic acid was added at 100 μM, FFAR4 agonist TUG891 was added at 100 μM, and FFAR1 agonist TUG424 was added at 100 μM for the first 2 days of differentiation. After 2 days of differentiation cocktail, media was changed to DMEM containing 10% FBS and 1 μg/mL insulin. Maintenance media was changed every 2-3 days for a total differentiation time of 4-8 days.

Mouse primary preadipocytes were grown to confluency in DMEM containing 10% FBS. Cells were not grown for another 2 days at confluency. Adipogenesis was induced using DMEM containing 10% FBS and differentiation cocktail consisting of insulin, dexamethasone, IBMX and/or DHA or TUG891. After 3 days of differentiation cocktail, media was changed to DMEM containing 10% FBS and 1 μg/mL insulin. Maintenance media was changed every 2-3 days for a total differentiation time of 4-8 days.

Human primary preadipocytes were grown to confluency in Growth Media (PromoCell). Adipogenesis was induced using Differentiation Media (PromoCell). After 3 days, media was changed to Nutrition Media (PromoCell) for another 12-14 days with media changes every 2-3 days.

Isolation of primary preadipocytes

Inguinal or epididymal white adipose tissue was removed and minced. Minced tissue was incubated in Collagenase Buffer (3,000 U/mL type II collagenase powder (Sigma, C6885), 100 U/mL DNase (Worthington, LS006344), 1 mg/mL poloxamer 188 (P-188) (Sigma P5556), 1 mg/mL BSA, 20 mM HEPES buffer, and 1 mM $CaCl_2$ in Medium 199 with Earle's salts (Sigma, M4530)) for 10min at 37C, followed by 20min shaking (250rpm) at 37C. Digested samples were strained through a 100 μm filter and diluted 1:1 in cell suspension buffer (2% FBS, 1 mg/mL P-188, and 1% pen/strep in PBS), followed by centrifugation (1300rpm, 5min).

For isolation of SVF cells depleted for RBCs and WBCs, the cell pellet was resuspended in cell suspension buffer and layered onto Histopaq-1077 (Sigma, 10771), followed by 20min centrifugation at 1300rpm. PBMC layer was removed and centrifuged (5min, 1300rpm), and cell pellet was resuspended in cell suspension buffer containing anti-CD45 microbeads (Miltenyi Biotec, 130-052-301) and anti-TER119 microbeads (Miltenyi Biotec, 130-049-901) for 30min at 4C, followed by MACS depletion using an LD column. Flow-through was collected and centrifuged (1300rpm, 5min). Cell pellet containing primary preadipocytes were resuspended in DMEM containing 10% FBS, 1% Pen/Strep, and 1% GlutaMAX.

For isolation of Lin^- ($CD45^-$ $CD31^-$ $TER119^-$) $CD34^+$ $CD29^+$ $SCA1^+$, the cell pellet post-digestion was resuspended in cell suspension buffer and stained with CD45 PE-Cy7 (eBioscience, 25-0451-81, 30-F11 clone, 1:800), CD31 PE-Cy7 (eBioscience, 25-0311-81, 1:800), TER119 PE-Cy7 (eBioscience, 25-5921-81, 1:800), CD34 Alexa Fluor 700 (eBioscience, 56-0341-82, 1:200), CD29 APC (eBioscience, 17-0291-80, 1:400), SCA1 Pacific Blue (Biolegend, 108120, 1:1000), propidium iodide for 20min, washed twice in cell suspension buffer, filtered and sorted on a FACSAria Fusion sorter.

To knock-out Ift88 in isolated primary preadipocytes, cells were sorted from $Ift88^{flox/flox}$ male mice for Lin^- ($CD45^-$ $CD31^-$ $TER119^-$) $CD34^+$ $CD29^+$ $SCA1^+$, and then plated on collagen-coated plates. Cells were grown to confluency and then transduced with an adenovirus expressing GFP only or GFP and Cre Recombinase (Vector BioLabs, 1060, 1700) at 3e7 PFU/cm^2 of plate surface area. After 48 h, cells were either differentiated, or trypsinized and plated onto a coverslip for differentiation or ciliation assays. GFP signal was amplified using an antibody against GFP and lipid droplets were visualized using LipidTox (Thermo, H34477, 1:200). Percent ciliation was determined by FGFR1OP (basal body) and ARL13B (axoneme) staining of GFP+ cells.

Sample preparation and immunoblot

Cells were lysed in 1x LDS buffer containing DTT and incubated at 95C for 5min. Proteins were separated using NuPage Novex 4%–12% Bis-Tris protein gels (Thermo Fisher Scientific, WG1402BOX) in NuPage MOPS SDS running buffer (50 mM MOPS, 50 mM Tris Base, 0.1% SDS, 1 mM EDTA, pH 7.7), followed by transfer onto nitrocellulose membranes (Life Technologies, LC2001) in Towbin Buffer (25 mM Tris, 192 mM glycine, pH 8.3) containing 10% methanol. Membranes were blocked in LI-COR Odyssey Blocking Buffer (LI-COR, NC9232238) for 30 min at room temperature, followed by incubation with primary antibody in blocking buffer for at least 1 h at room temperature. The membrane was washed 3 times for 10min in TBST buffer (20 mM Tris, 150 mM NaCl, 0.1% Tween 20, pH 7.5) at room temperature, incubated with secondary IRDye antibodies (LI-COR) in blocking buffer for 30 min at room temperature, and then washed 3 times for 10min in TBST buffer. Membranes were scanned on an Odyssey CLx Imaging System (LI-COR), with protein detection at 680 and 800 nm. Antibodies were used as follows: TULP3 (Yenzym, 1:500), PPARγ (Cell signaling, 2435, 1:1000), Tubulin (Sigma, 9026, 1:5000), CEBPα (Cell signaling, 8178, 1:1000), CTCF (Cell signaling, 2899, 1:1000), ERK (Cell signaling, 9107, 1:1000), pERK (Cell signaling, 9101, 1:1000), AKT (Cell signaling, 9272, 1:1000), pAKT (Cell signaling, 9271, 1:1000), CREB (Cell signaling, 9104, 1:1000), pCREB (Cell signaling, 9198, 1:1000)

Glucose and serum analysis

To measure glucose levels, a small drop of blood from the tail was placed on a human glucometer (Bayer). Food was removed in the late afternoon and fasting glucose levels measured the next day. To minimize stress, mice were handled for one week to acclimate. For serum analysis, blood was collected via cardiac puncture and serum harvested. ELISAs for insulin (ALPCO, 80-INSMSU-E01), leptin (ALPCO, 22-LEPMS-E01) and free fatty acids (Wako, NEFA-HR2) was done according to manufacturer's instructions. Data were plotted in GraphPad.

Oil red O staining for lipid visualization and quantification

Cells are fixed in 4% PFA/PBS for 10min at room temperature, followed by 3 rinses in PBS. Samples were incubated in 60% isopropanol for 5min at room temperature and then allowed to dry completely. Samples are then incubated in freshly diluted 60% Oil Red O staining solution in water (stock is 0.5% Oil Red O (Sigma, 00625) in isopropanol) for 20min at room temperature, followed by 3 rinses in water. Samples were allowed to dry completely and imaged.

For quantification, Oil Red O was extracted by incubating dried samples stained on the same day in 100% isopropanol for 5min at room temperature and absorbance was measured at 510nm.

To visualize lipids in liver tissue section, liver samples were fixed in 4% PFA for 2 h at 4C, cryprotected in 30% sucrose overnight before cyrosectioning. Tissue sections were air-dried, before staining was performed. Slides were mounted with FluoroMount G before visualized. To quantify the area occupied by Oil Red O, images were converted to binary images using the Threshold function and quantified using the Analyze Particle function in ImageJ.

Live Cell Imaging Analysis for adipogenesis and proliferation

Live imaging for kinetics quantification of adipogenesis and for proliferation assay was performed using the IncuCyte Live Cell Analysis Imaging System (Essen Bioscience) with images acquired every 2 h using the 10x objective. Proliferation was assessed using a confluency mask generated by the IncuCyte Zoom Analysis Software using phase images. For the kinetic quantification of adipogenesis, 3T3-L1 cells were differentiated as described above and supplemented with 200nM BODIPY 493/503, and green fluorescence images were acquired every 2 h using default IncuCyte setting. Total green fluorescence intensity was determined from a green fluorescent mask generated by the IncuCyte Zoom Analysis Software.

Echo-MRI and CLAMS

To assess fat versus lean mass, whole composition analysis was performed using the EchoMRI-3in1 machine from Echo Medical System according to manufacturer's instructions. To assess any changes in metabolism, we used the Comprehensive Lab Animal Monitoring System (CLAMS) made by Columbus Instruments, Inc. In brief, mice were single-housed in a large enclosure with precise control over the temperature and light / dark cycle. All values are normalized to body weight. Data were analyzed using the CLAX software from Columbus Instruments, exported into Excel and plotted in GraphPad.

Quantitative Real time PCR

RNA was extracted using the RNeasy Lipid Tissue Kit (QIAGEN) and cDNA was synthesized using M-MLV Reverse Transcriptase (Invitrogen, 28025-013). Quantitative real time PCR was performed using TaqMan Probes (Invitrogen) and the TaqMan Gene Expression Master Mix (Applied Biosystems, 4369016) in 96-well MicroAmp Optical reaction plates (Applied Biosystems, N8010560). Expression levels were normalized to the average expression of the housekeeping gene *NoNo*.

For Figures S2A and S2H, whole white or brown adipose tissue was placed in in TRIzol (Thermo Fisher) and disrupted using the TissueLyser LT (QIAGEN) and RNA was isolated using the QIAGEN RNeasy kit. cDNA was synthesized using the qScript cDNA synthesis kit (Quantabio). RT-qPCR was performed in technical triplicates on a Quant Studio 6 real-time PCR machine (Applied Biosystems) using the PowerUp master mix (Invitrogen). Fold changes were calculated using the $2^{-\Delta\Delta CT}$ method (Schmittgen and Livak, 2008) and expression levels normalized to the average of the housekeeping genes *Hprt* and *Pde12*.

EdU incorporation for cell cycle analysis

EdU incorporation was assessed using the Click-iT EdU Imaging Kit (Thermo, C10340) according to manufacturer's recommendation. Briefly, 3T3-L1 were grown to confluency in a 96-well cell imaging plate (Eppendorf, 0030741013) and kept at confluency for 2 days. Differentiation was initiated using the differentiation cocktail indicated in the figure legend, and EdU was added for a final concentration of 1 μM after 16 h of differentiation. After a total of 40 h of differentiation, cells were fixed in 4% PFA/PBS for 15min at room temperature, followed by 2 rinses in 3%BSA/PBS. Cell were permeabilized in 0.5% Triton-X/PBS for 20min at room temperature, followed by 2 rinses in 3%BSA/PBS. Samples were then incubated in freshly made Click-iT reaction cocktail for 30min at room temperature, followed by 1 rinse in 3%BSA/PBS and 1 rinse in PBS. Samples were then incubated in 2 μg/mL Dapi in PBS for 30min at room temperature followed by 1 rinse in PBS. Samples were stored in PBS and images were acquired using a Keyence fluorescent microscope (10x objective). EdU positivity was assessed using the CellProfiler pipeline.

Live Cell Ciliary cAMP assay

3T3-L1 cells were seeded at 1e4 cells/well in a 96-well cell imaging plate (Eppendorf, 0030741013) and transduced the following day with the ratiometric cilia-targeted cADDis BacMam (Molecular Montana, D0211G) according to manufacturer's recommendation. Briefly, cell were infected with 25ul of BacMam sensor stock in a total of 150ul of media containing 2mM Sodium Butyrate (Molecular Montana) for 30min at room temperature followed by 6 h in the 37C tissue culture incubator. BacMam was removed and replaced with DM containing 1mM Sodium Butyrate for 16-24 h. Prior to imaging, cells were incubated in PBS for 20min at room temperature. Images were acquired on a Marianas spinning disk confocal (SDC) microscopy (Intelligent Imaging Innovations) (40x, epi-fluorescence) every 10 s for 5min with agonist added after 30sec. Red fluorescence was used to determine a mask and background subtracted green and red fluorescent intensity over time was determined using Slidebook (Intelligent Imaging Innovations).

PPARγ reporter cell line generation

The donor plasmid containing a 5′ homology arm (with stop codon mutated), T2A, EGFP, and 3′ homology arm was generated by Gibson Assembly of pUC19 plasmid linearized by BamHI and EcoRI digestion, Gibson fragment 1 (GCTTGCATGCCTGCAGGTC GACTCTAGAGGACCCCTCCAAAGTGAAGCAGTCTTTTATCTTGCTGGTAATGGGATGTGTTTGTGCTAAGCAAAAAAACAGCAAGG CTTACACTTGAAAAATCTTATTTGAAGCTGTTATGAGAATGTAGGTAGAAGTTTAAAAAGGAAAACAAAATAAAACAAAACAAAAACA AACAAACAAACAAAACACTCCTCCAGGAGCAAAGGTTGGTAATGTGATTTCTGTGAGGAGAAGCATGTTGCCAGAAGAGGCCTTG GGTTGAAGACAGGATGCTCCTGATGGCATTGCATCAGTTAGTCCTGGTTGGGAAGGGCTTGAGCCTTTGATTCCATCCTTGGGTC TTGCCCATTAGCTGCAGAGCCTCGCTCCACGAACCTGCTTAAGAAACAGGGCGGTGATGGGGTCTTGGCTCTTCGGTAAAGCAT GTGCCTAACAGCTCGAGAACTGGGTTTCTTCTCCAGCCTGGGGAGCAGGGAATCTGAAGCTGCACTCCTTAGAGCCCCAGAGGA GGTCTGACAAAGCCTCTTTTTGTCTTCTCATTCTCCCAGACCGCCCAGGCTTGCTGAACGTGAAGCCCATCGAGGACATCCAAGA CAACCTGCTGCAGGCCCTGGAACTGCAGCTCAAGCTGAATCACCCAGAGTCCTCTCAGCTGTTCGCCAAGGTGCTCCAGAAGAT GACAGACCTCAGGCAGATCGTCACAGAGCACGTGCAGCTACTGCATGTGATCAAGAAGACAGAGACAGACATGAGCCTTCACCC CCTGCTCCAGGAGATCTACAAGGACTTGTATTTGCAGGAAAGTCCCGGCTCCGGAGAGGGCAGAGGAAGTCTGCTAACATGCGG TGACGTCGAGGAGAATCCTGGCCCAATGGTGAGCAAGGGCGAGGAGCTGTTCACCGGGGTGGTGCCCATCCTGGTCGAGCTGG ACGGCGACGTAAACGGCCACAAGTTCAGCGTGTCCGGCGAGGGCGAGGGCGATGCCACCTACGGCAAGCTGACCCTGAAGTTC ATCTGCACCACCGGCAAGCTGCCCGTGCCCTGGCCCACCCTCGTGACCACCCTGACCTACGGCGTGCAGTGCTTCAGCCGCTA CCCCGACCACATGAAGCAGCACGACTTCTTCAAGTCCGCCATGCCCGAAGGCTACGTCCAGGAGCGCACCATCTTCTTCAAGGA CGACGGCAACTACAAGACCCGCGCCGAGGTGAAGTTCGAGGGCGACACCCTGGTGAACCGCATCGAGCTGAAGGG) and Gibson fragment 2 (CGAGGGCGACACCCTGGTGAACCGCATCGAGCTGAAGGGCATCGACTTCAAGGAGGACGGCAACATCCTGGGGCA CAAGCTGGAGTACAACTACAACAGCCACAACGTCTATATCATGGCCGACAAGCAGAAGAACGGCATCAAGGTGAACTTCAAGATCC GCCACAACATCGAGGACGGCAGCGTGCAGCTCGCCGACCACTACCAGCAGAACACCCCCATCGGCGACGGCCCCGTGCTGCTG CCCGACAACCACTACCTGAGCACCCAGTCCGCCCTGAGCAAAGACCCCAACGAGAAGCGCGATCACATGGTCCTGCTGGAGTTC GTGACCGCCGCCGGGATCACTCTCGGCATGGACGAGCTGTACAAGTAATTCTATTGATTGCACTATTATTTTGAGGGAAAAAAATCT GACACCTAAGAAATTTACTGTGAAAAAGCATTTAAAAACAAAAAGTTTTAGAACATGATCTATTTTATGCATATTGTTTATAAAGATACAT TTACAATTTACTTTTAATATTAAAAATTACCACATTATAAAATTGTTTATAGTATTTAAAGAATGAATGCATGTCTCCCATTCTGCCATCAC AGATGGGGGAAAGGATTTCCTCATTTTATTTCTTTTCTTCTTTCTTTTCTTCATCCTTTGACATGCATATGTGCTCATATATATGTTTATG TGTGAGTAGATGCTGTGTATGTGTATGGAGGCCCAGAGACAGCTCTAAAGCTGGCTCATTCTCAGGACTGTCATCTACCCACTTTTA GACAGGGTCTTTCATTTGGCCTAAATTTAACCAATTAGGTTAGACTAGAGGGTCAGTGAGCCCCGGGGAACGGCCTGGCCCCACCC GCCCATCACTACCCTGTCTGGCATGTTTAGGTGGATTCGAGAGGAGGGGAGGAGCTGGACTCAGGTCCTCATGCTCTCAAGGCTTC ACAAGAACCCAAACTTCTCCCACGACTCTGAGTTTTCACGAATCACCAGCAACATGTTTAACATATTGTCATCCCTCTATACTCATGG GGTCTGGCTCCAGGCCTCCTGAAGGAGCCATGGGTGTTCAAGTTTTCATAACAGGAGTTTCAAGTAAACTCTGCATACTGTCCCCTA TCCTTTGAACTGTCTCTAGATACCTACAATACCTAACACAATGGAAATGTTGCACTGGCCGTCGTTTTACAACGTCGTGAC).

A p306 plasmid containing a sgRNA (GGAACACGTTGTCAGCGGGT) targeting the 3′UTR of *Pparγ* was generated by annealing the top and bottom oligos (TTGGGAACACGTTGTCAGCGGGTGTTTAAGAGC and TTAGCTCTTAAACACCCGCTGACAACGTGTTC CCAACAAG) and ligating into BlpI/BstXI digested MCB306.

3T3-L1 Cas9-BFP cells were co-transfected with p306 sgPparγ and donor plasmid, sorted for GFP positivity (from p306 plasmid) 48 h post-infection and allowed to grow for 10 days. 100 GFP negative cells (since expression was transient) were sorted into each well of a 96 well plate and allowed to grow. Cells were duplicate plated and one set was induced to differentiate using the traditional DM(1 μg/mL insulin, 1 μM dexamethasone, 0.5mM IBMX) in the IncuCyte live-imaging system to identify wells containing cells that became GFP positive during adipogenesis. Cells in positive wells were single cell sorted, allowed to grow, duplicate plated, and differentiated in the IncuCyte live-imaging system. In total, we obtained 5 3T3-L1 PPARγ T2A reporter cell lines.

Next generation RNA sequencing and analysis

3T3-L1 cells were grown to confluency, kept confluency-arrested for 2 days, and differentiated in triplicates using historical DM, ctrl (-DHA) differentiation cocktail, or DHA cocktail. After 24 h, RNA was extracted using the QIAGEN RNeasy kit, followed by library construction. Sequencing data was generated on an Illumina HiSeq4000 (purchased with funds from NIH under award number S10OD018220).

Sequencing data QC was performed using fastqc and trimmomatic. Differential gene expression compared to undifferentiated (0 h) was assessed using three pipelines: Kallisto (reference refseq), followed by sleuth; Star (reference gencode) followed by cutdiff; and star (reference gencode) followed by htseq and deseq2. Differential gene expression was called significant if q-value < 0.05 for all three pipelines.

ATACseq and TF motif enrichment analysis

3T3-L1 cells were grown to confluency, kept confluency-arrested for 2 days, and in duplicates left untreated, treated with 100 μM DHA, or treated with 1 μM Dex for 4 h. Aliquots of 70,000 to 80,000 cells were taken and processed as previously described (Corces et al., 2017). Briefly, 200 U/mL DNase (Worthington Biochemical, NJ, USA) were added to the cell aliquot and incubated at 37C for 30 min, centrifuged at 500 g for 5 min at room temperature and resuspended in 1 mL cold PBS. Resuspended samples were centrifuged at 500 g for 5 min at 4C and washed in 500 μl cold RSB buffer (10 mM Tris-HCl pH 7.4, 10 mM NaCl, and 3 mM $MgCl_2$) followed

by centrifugation at 500 g for 5 min at 4C. Samples were resuspended and lysed for 3 min on ice in 50 μl RSB buffer containing 0.01% Digitonin (Promega, WI, USA), 0.1% NP40 and 0.1% Tween20. After lysis, 950 μl RSB with 0.1% Tween20 were added to the sample and mixed by inverting. Samples were centrifuged at 500 g for 5 min at 4C, resuspended in 50 μl of transposition mix (25 μl TD buffer [Illumina], 2.5 μl Tn5 [Illumina], 16.5 μl PBS, 0.5 μl 1% Digitonin, 0.5 μl 10% Tween20 and 5 μl water) and incubated at 300 rpm at 37C. All samples were purified using MinElute PCR Purification columns (QIAGEN, Germany) and amplified and barcoded with custom Nextera primers (Table S5) as previously described (Buenrostro et al., 2015). ATAC libraries were paired-end sequenced (2x 76 bp) on a NextSeq500 (Illumina) using a high output v2 150 cycle kit (Illumina).

BCL files were demultiplexed using bcl2fastq (Illumina), adapters were trimmed using cutadapt and reads were aligned to the mouse genome (mm9) using bowtie2. Duplicates were removed using Picard MarkDuplicates. Mitochondrial reads and reads mapping to a modified version of the mm9 ENCODE blacklist (Table S6) were removed using samtools. Peaks were called using MACS2 and filtered by q value for the top 100K peaks. The peak set was then reduced to non-overlapping peaks and peak width was adjusted to 500 bp. Transcription factor motif analysis was performed using chromVAR. Bias-corrected deviations were plotted for the 50 most variable transcription factor motifs using the R pheatmap package.

Filtered and normalized enhancer regions from (Siersbaek et al., 2017) were intersected with CTCF-binding sites from atac-seq. The resulting data was further filtered to keep only enhancer sites that were also detected by CTCF CHIP-seq from (Siersbaek et al., 2017). Corresponding promoter sites were used to infer genes regulated by these promoters.

QUANTIFICATION AND STATISTICAL ANALYSIS

Statistical parameters including the statistical test used, exact value of n, what n represents, and the distribution and deviation are reported in the figures and corresponding figure legends. Most data are represented as the mean ± standard deviation and the p value was determined using two-tailed Student's t tests.

Unless otherwise stated, statistical analyses were performed in Microsoft Excel and GraphPad Prism.

DATA AND CODE AVAILABILITY

The accession number for the ATACseq data of 3T3L1 cells undergoing differentiation reported in this paper is GEO: GSE118470. The accession number for the RNaseq data of 3T3L1 cells undergoing differentiation reported in this paper is GEO: GSE118471.

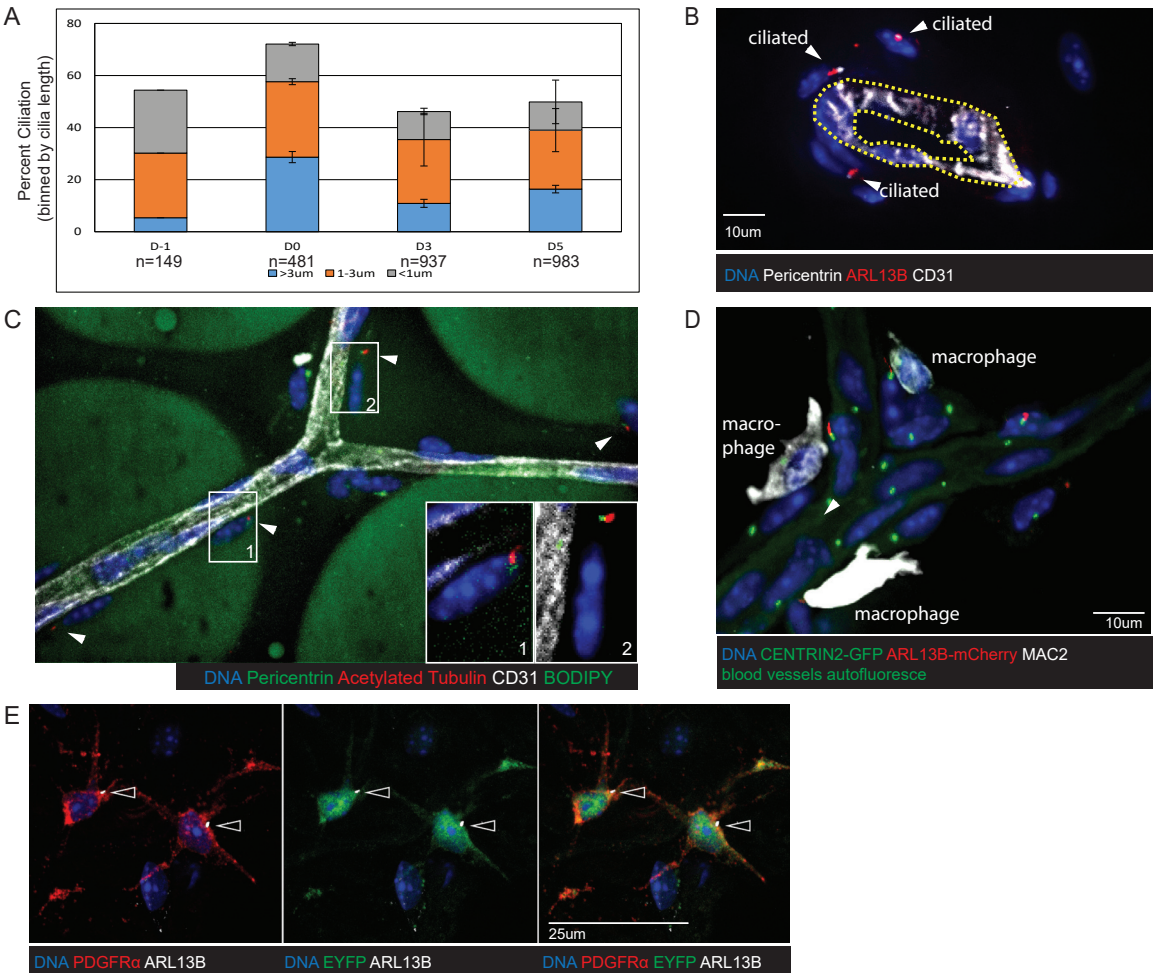

Figure S1. Preadipocytes Are Ciliated *In Vivo* and Located in the Perivascular Niche Adjacent to Macrophages, Related to Figure 1

(A) Primary preadipocytes in the SVF (depleted for RBCs and WBCs) from the inguinal WAT of CENTRIN2-GFP, ARL13B-mCherry (*cilia glow*) mice were differentiated using the historical DM (1 μg/ml insulin, 1 μM dexamethasone, 0.5mM IBMX). Ciliation status was quantified for different differentiation time points (D-1 refers to Day −1 when cells are not confluent (1 day post-isolation), D0 refers to Day 0 when cells are confluent and differentiation is initiated, D3 refers to Day 3 of differentiation when cells are switched into maintenance media (1 μg/ml insulin), and D5 refers to Day 5 of differentiation when lipid starts being accumulated). n = number of cells quantified per time point; cilia are categorized by length of axoneme since there was a wide range of ciliary lengths; bar graphs are average number of ciliated cells ± SD

(B) Cross-section of a blood vessel in epididymal WAT from a wild type mouse shows that ciliated cells are perivascular. Yellow dotted line outlines blood vessel as determined by Cd31 staining.

(C) Whole mount image of epididymal WAT from wild type mouse. BODIPY visualizes lipid droplets. Arrow heads point to ciliated perivascular cells. CD31 visualizes blood vessels, pericentrin visualizes the ciliary base, and acetylated tubulin or ARL13B visualize the ciliary axoneme.

(D) Whole mount image of epididymal WAT from *cilia glow* mouse showing that perivascular macrophages as visualized by MAC2 staining are not ciliated.

(E) Immunofluorescence for preadipocytes (PDGFRα, red), cilia (ARL13B, marked by arrowheads) and lineage tracer (EYFP, green) 5 weeks post induction of lineage label in *Pdgfrα-CreERT Rosa26*^{EYFP} mice. Scale bar is 25 μm.

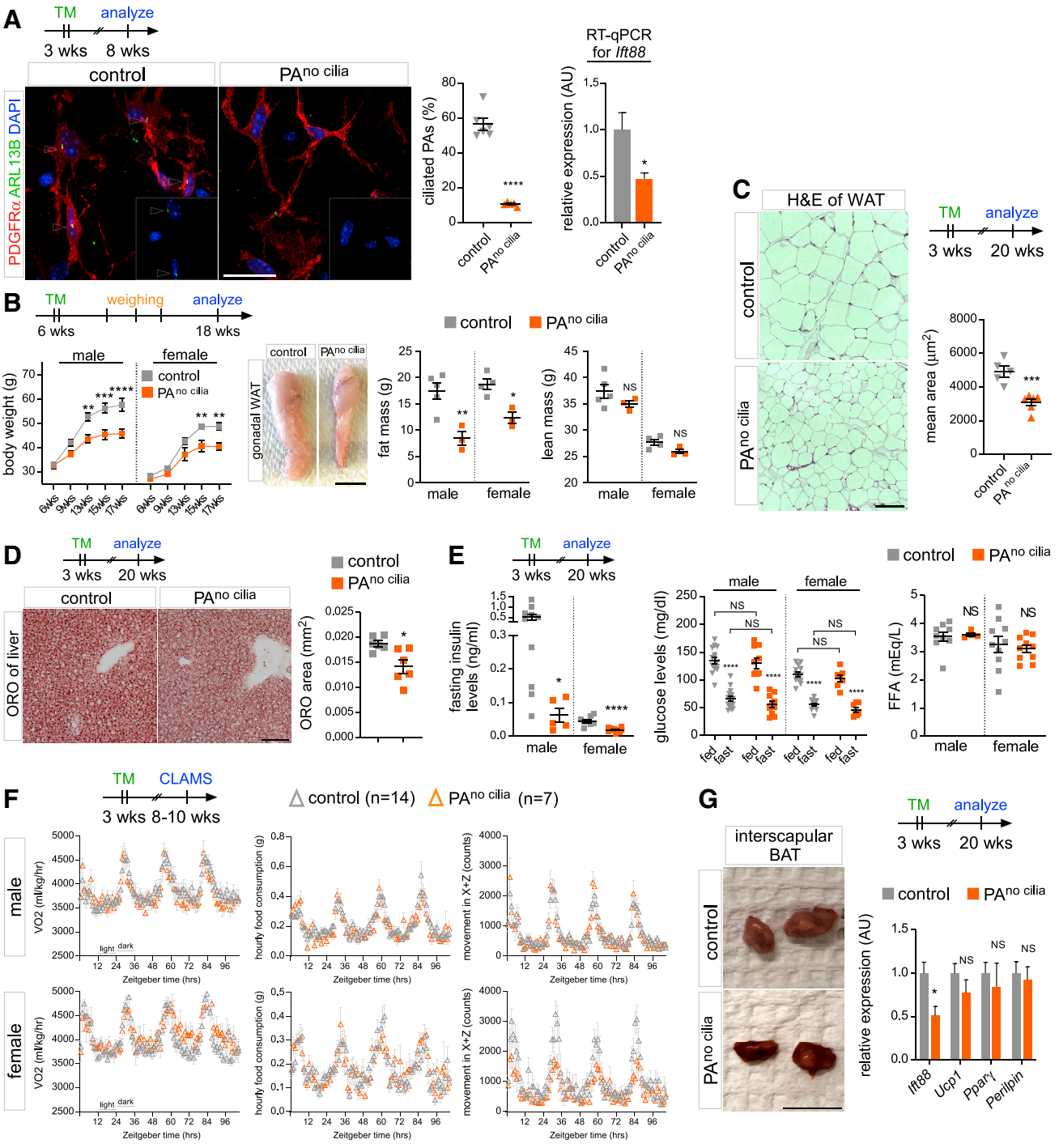

Figure S2. Loss of Preadipocyte Cilia Has a Profound Effect on WAT Expansion, Related to Figure 2

(A) Left: Immunofluorescence for preadipocytes (PDGFRα, red) and cilia (ARL13B, green) 5 weeks post tamoxifen administration in control and PA$^{no\ cilia}$ mice. Ciliated PAs are marked by arrowheads, DAPI stains nuclei. Scale bar is 25 μm. Right: Quantifications of the percentage of ciliated PAs present 5 weeks after conditional removal of PA cilia. Far right: Comparison of *Ift88* expression between control and PA$^{no\ cilia}$ mice via RT-qPCR from whole gonadal WAT (n = 4 per genotype).

(B) Left: Body weight measurements in control and PA$^{no\ cilia}$ mice (n = 4 for control and n = 3 for PA$^{no\ cilia}$ mice). Right: Picture of gonadal fat pad and Echo-MRI measurements of total fat and lean mass in control and PA$^{no\ cilia}$ mice 11 weeks after tamoxifen administration. Scale bar is 1cm.

(C) H&E staining of gonadal WAT tissue sections and the respective quantifications of the mean area of adipocytes in control and PA$^{no\ cilia}$ mice. Scale bar is 100 μm.

(legend continued on next page)

(D) Left: Oil Red O-stained liver sections from control and PA$^{no\ cilia}$ mice. Right: Quantification of area occupied by Oil Red O between genotypes. Scale bar is 100 μm.

(E) Serum levels for insulin and free fatty acids (FFA) were measured using ELISA and glucose levels using a glucometer between control and PA$^{no\ cilia}$ mice at either fed state or after an overnight fasting period as indicated.

(F) Plotting of hourly oxygen consumption (VO2), food intake and total movement over 4 days of control (n = ♂14 & ♀12) and PA$^{no\ cilia}$ mice (n = ♂7 & ♀9).

(G) Dissected interscapular brown adipose tissue (BAT) of two control and two PA$^{no\ cilia}$ mice. Scale bar is 1 cm. Comparison of *Ift88*, *Ucp1*, *Pparγ* and *Perilipin* expression between control (n = 6) and PA$^{no\ cilia}$ mice (n = 5) via RT-qPCR from whole interscapular BAT. All data are represented as mean ± SEM p values were calculated using standard t test and two-way ANOVA followed by Tukey's multiple comparison test (*<0.05, **<0.01, ***<0.001 and ****<0.0001). Of note, all mice depicted are littermates and maintained on breeder chow starting the day of tamoxifen administration.

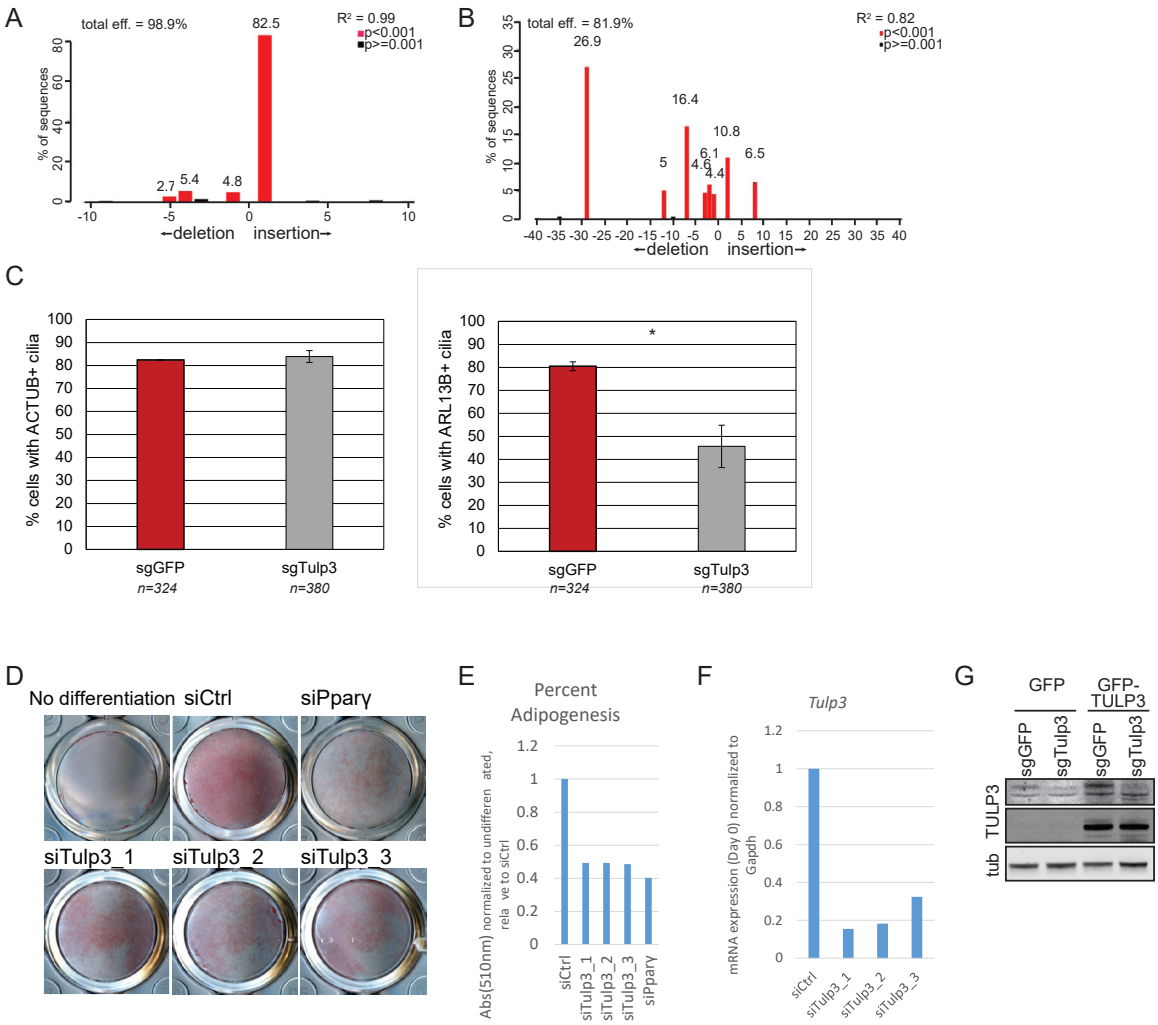

Figure S3. Ciliary GPCRs Are Required for Adipogenesis, Related to Figure 3

(A) TIDE analysis showing genomic alterations in the engineered 3T3-L1 sgTulp3 cell line.

(B) TIDE analysis showing genomic alterations in the engineered 3T3-L1 sgFfar4 cell line.

(C) Loss of TULP3 has no effect on ciliary structure, as determined by acetylated tubulin staining, but prevents trafficking of ciliary proteins, including ARL13B.

(D) Loss of TULP3 using siRNA-mediated knockdown results in attenuated adipogenesis. 3 different siRNAs targeting TULP3 were used, siRNA targeting PPARγ is positive control. Lipid accumulation visualized by Oil Red O staining

(E) Quantification of adipogenesis by isopropanol extraction of Oil Red O.

(F) Quantification of TULP3 knockdown efficiency using siRNA.

(G) Immunoblot showing depletion of TULP3 in 3T3-L1 sgTulp3 cell line, and overexpression of GFP-TULP3 fusion protein. p values calculated using t test, * $p < 0.05$;

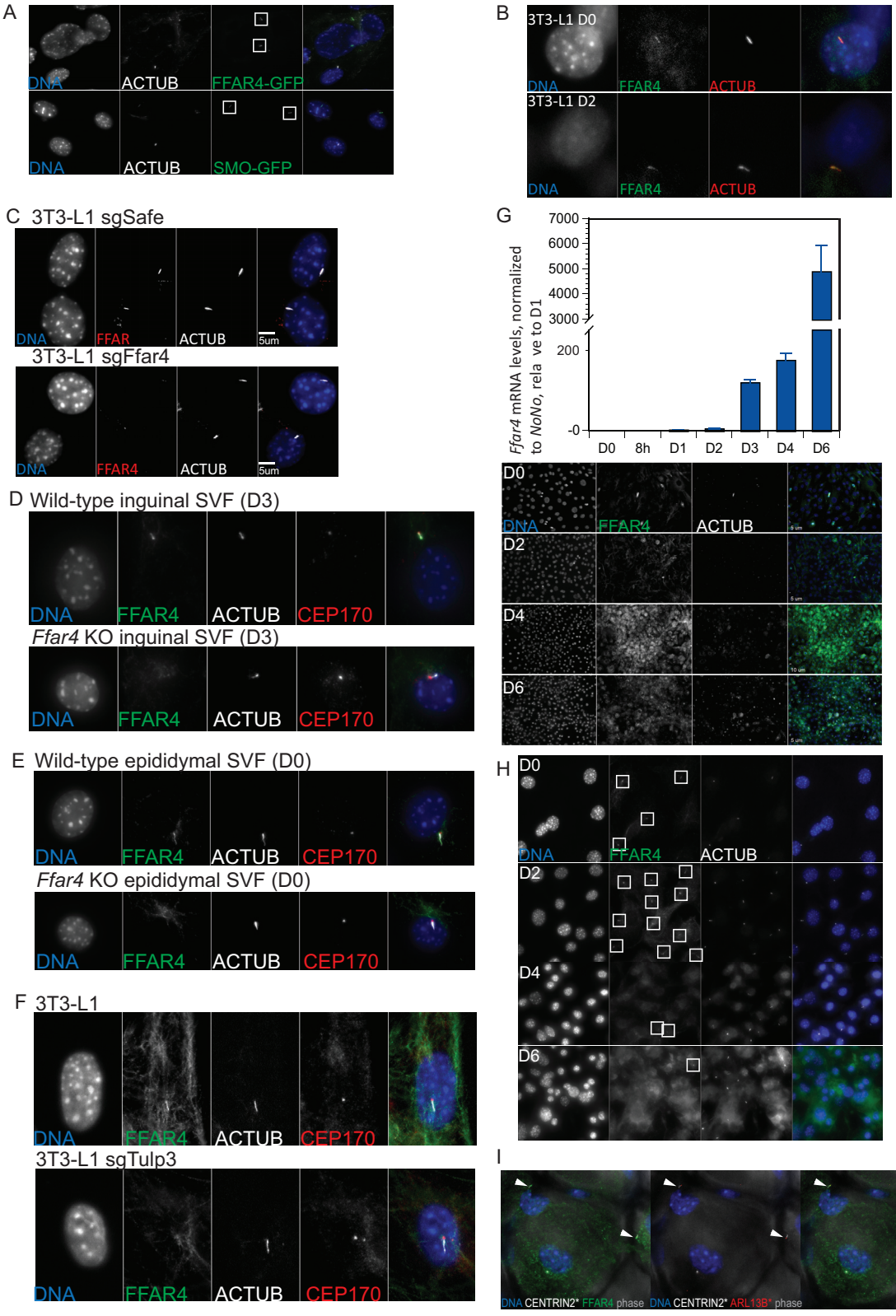

(legend on next page)

Figure S4. FFAR4 Is a Novel Ciliary GPCR Displayed by Preadipocytes, Related to Figure 4

(A) 3T3-L1 FFAR4-GFP fusion protein localizes to primary cilium. SMO-GFP is positive control.

(B) Validation of ciliary localization of FFAR4 using second independent antibody (Santa Cruz). 3T3-L1 cells on Day 0 and Day 2 of differentiation.

(C-E) Validation of FFAR4 antibody in (C) 3T3-L1 cells using Crispr/Cas9, (D) SVF isolated from inguinal and (E) epididymal white adipose tissue of wild-type and *Ffar4* knockout littermates. We note that there is some non-specific ciliary FFAR4 background staining with this antibody.

(F) Representative immunofluorescence images showing depletion of ciliary FFAR4 with loss of TULP3 protein.

(G) FFAR4 expression by mRNA and protein increases during differentiation. 20x objective was used to visualize the whole cell. This makes visualization of individual cilia difficult.

(H) Endogenous FFAR4 is ciliary during 3T3-L1 differentiation. D0, 2, 4, 6 are Day 0, 2, 4 and 6 of differentiation.

(I) Endogenous FFAR4 localizes to the primary cilium of preadipocytes and to the plasma membrane of mature adipocytes *in vivo* in epididymal WAT whole mounts from *cilia glow* male mice. The fluorescence intensity of FFAR4 localized to the primary cilia is higher than the fluorescence intensity of FFAR4 localized to the adipocyte plasma membrane, consistent with FFAR4 receptor density being higher in the primary cilium. White arrows and boxes highlight cilia.

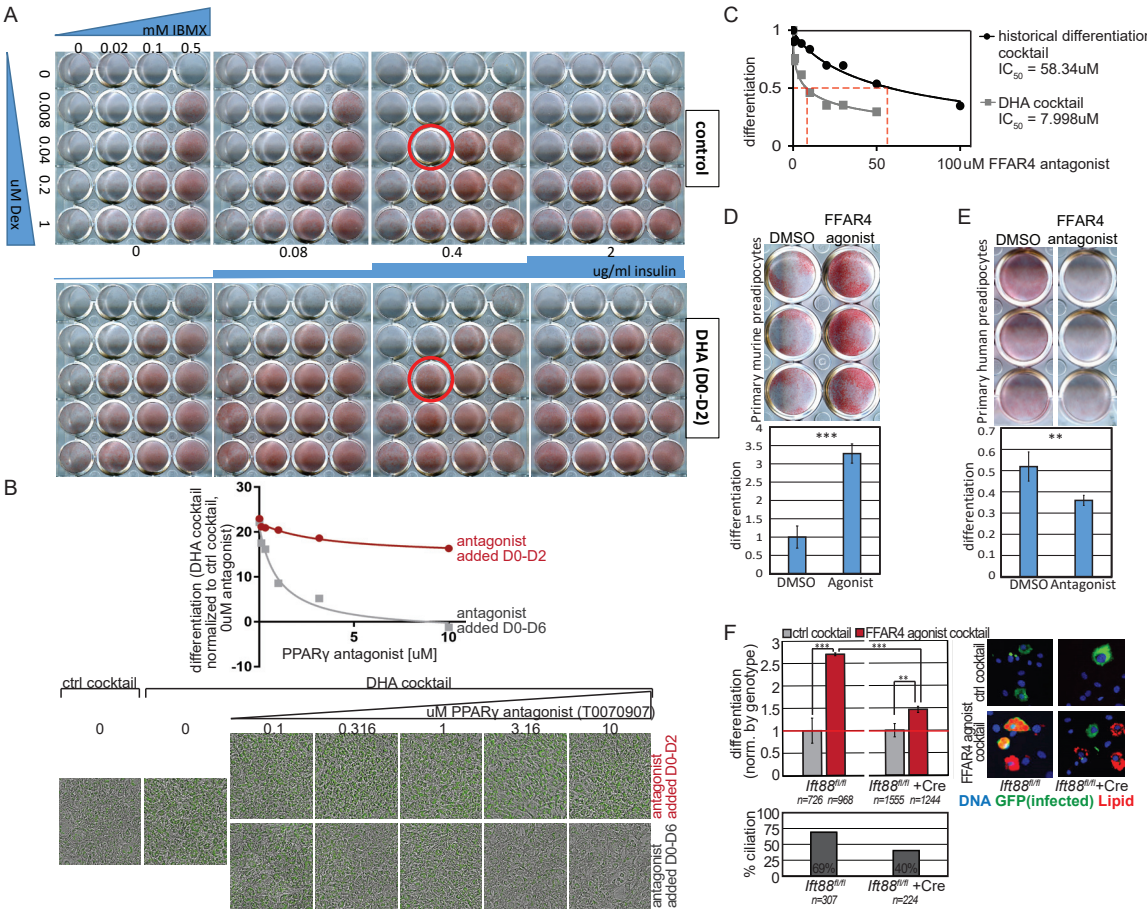

Figure S5. FFAR4 Activation Promotes Adipogenesis, Related to Figure 5

(A) DM component titration in the presence or absence of 100 μM DHA to determine the optimal concentrations of insulin, dexamethasone, and IBMX to observe enhancement of differentiation by DHA. DHA and DM components were added for 48h to 2 day post-confluent 3T3-L1 cells. At 0.4 μg/ml insulin, 0.02mM IBMX, 0.04 μM dexamethasone (red circle), there is little differentiation with EtOH control and robust differentiation in the presence of DHA, as visualized by Oil Red O.

(B) DHA does not promote adipogenesis by directly activating PPARγ. 3T3-L1 preadipocytes were differentiated using the DHA cocktail for 2 days followed by maintenance media (1 μg/ml insulin) for 4 days. Lipid accumulation was assessed by green fluorescent BODIPY dye. The PPARγ antagonist T0070907 was added either concurrently with DHA (D0-2) or throughout the differentiation time course (D0-6). Presence of the PPARγ antagonist throughout the differentiation time course (D0-6) inhibits adipogenesis in a dose-dependent manner, consistent with PPARγ being required during the second phase of adipogenesis. The presence of the PPARγ concurrently with DHA (D0-2) does not inhibit adipogenesis, arguing that DHA does not promote adipogenesis by directly activating PPARγ.

(C) FFAR4 antagonist (AH7614) has a lower IC_{50} when 3T3-L1 adipogenesis is induced by DHA cocktail versus historical DM.

(D) Addition of FFAR4 agonist TUG891 (100 μM) during the first 72h of differentiation enhances differentiation of primary murine preadipocytes in the SVF from inguinal WAT.

(E) Addition of FFAR4 antagonist AH7614 (10 μM) to differentiating human preadipocytes during the first 72h attenuates differentiation.

(F) FFAR4 activation promotes adipogenesis of primary mouse preadipocytes via the primary cilium. Preadipocytes (Lin^-, $CD34^+$, $SCA1^+$, $CD29^+$) isolated from *Ift88*$^{flox/flox}$ males were transduced with an adenovirus expressing GFP only or GFP and Cre recombinase (+Cre). IFT88 is required for ciliation and percent ciliation was determined by FGFR1OP (basal body) and ARL13B (axoneme) staining of GFP+ confluent preadipocytes. Percent differentiation was determined by LipidTox Neutral Red staining of GFP+ cells differentiated with modified cocktail in the presence or absence of 100 μM TUG891. Representative images shown. n = number of GFP+ cells counted. Differentiation data is normalized to ctrl ± SD. ** $p < 0.01$; *** $p < 0.001$.

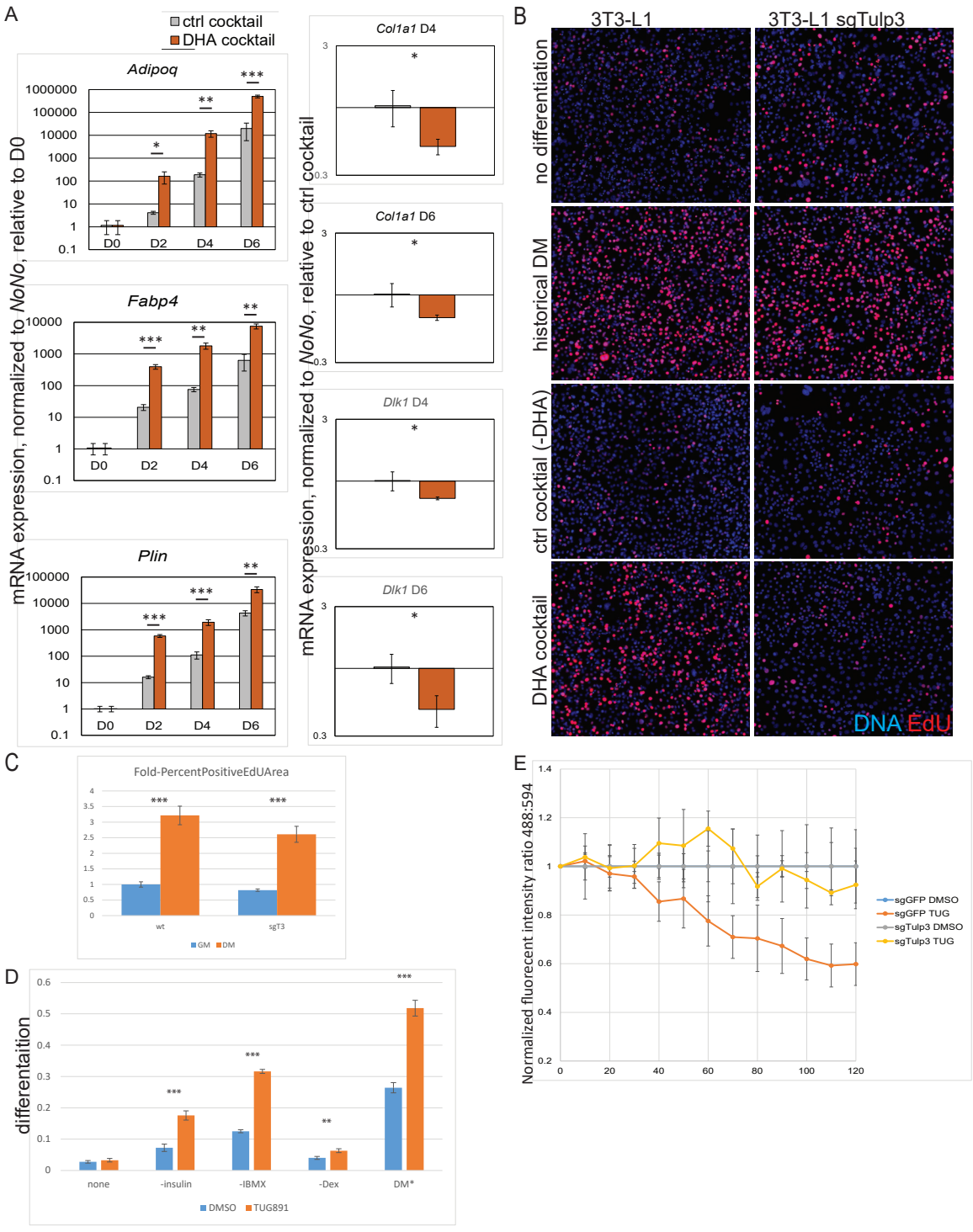

Figure S6. FFAR4 Regulates Initiation of Adipogenesis via cAMP, Related to Figure 6

(A) DHA cocktail promotes activation of adipogenic genes Adiponectin, Fabp4, and Plin1, and represses expression of preadipocyte genes Col1a and Dlk1. These data show that DHA cocktail initiates adipogenesis of 3T3-L1 preadipocytes. Bar graph is average of three independent experiments ± SD

(B) DHA cocktail results in cell cycle re-entry and this is dependent on Tulp3 protein. Representative images showing EdU incorporation of confluency-arrested 3T3-L1 cells maintained in growth media, or differentiated using the historical DM, the ctrl cocktail (-DHA), or the DHA cocktail. EdU was added at 16h, and cells were fixed and stained at 40h.

(legend continued on next page)

(C) Addition of historical DM (1 μg/ml insulin, 1 μM dexamethasone, 0.5mM IBMX) to 3T3-L1 cells lacking Tulp3 promotes cell cycle re-entry. Tulp3 protein is only required for DHA-mediated mitotic differentiative expansion and adipogenesis.

(D) Quantification of adipogenesis in the presence or absence of FFAR4 agonist with one component of the modified cocktail omitted per condition. Images shown in Figure 5B. FFAR4 agonist can partially substitute for Dex, insulin, and IBMX, but has quantitatively the largest effect replacing IBMX. This suggests that FFAR4 activation results in elevation of cAMP second messenger. This can enhance adipogenesis in the absence of any single cocktail component, but has the greatest effect replacing the phosphodiesterase inhibitor IBMX.

(E) Loss of Tulp3 prevents increase in ciliary cAMP by addition of FFAR4 agonist. cAMP sensor with red fluorescent constitutive ciliary marker was expressed in 3T3-L1 sgGFP (wild type control) and sgTulp3 cells. Addition of FFAR4 agonist, but not DMSO control, in wildtype but not Tulp3 knockout cells results in a significant decrease in the ratio of green fluorescence (cAMP sensor) to red fluorescence (constitutive ciliary marker) intensities, showing that FFAR4 activation elevates ciliary cAMP and that this is dependent on Tulp3 and thus ciliary localization of FFAR4. Bar graphs represent mean ± SD. *<0.05; ** $p < 0.01$; *** $p < 0.001$.

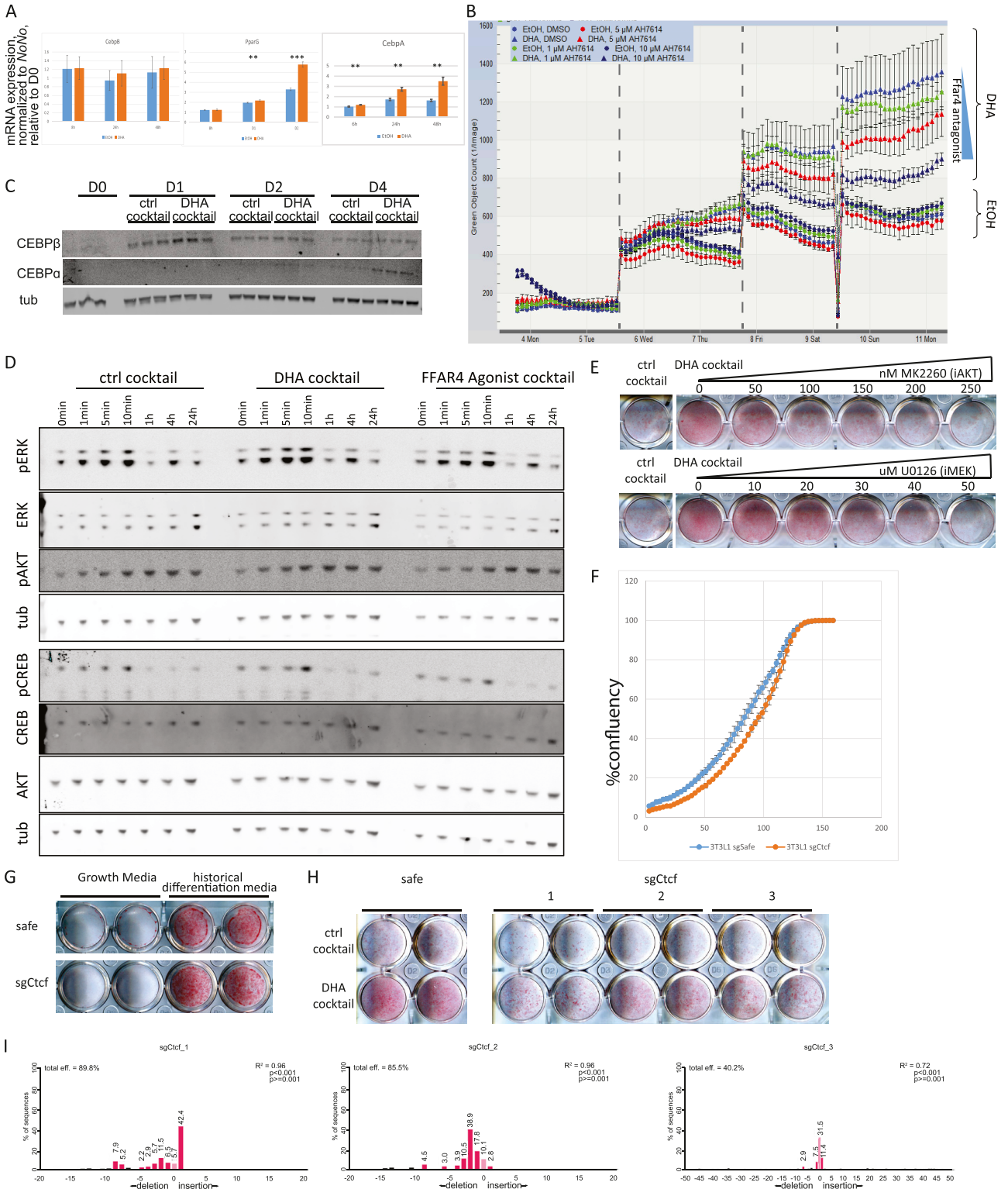

(legend on next page)

Figure S7. FFAR4 Activates the Master Adipogenic Transcription Factors PPARγ and CEBPα via CTCF-Dependent Genome-wide Reprogramming, Related to Figure 7

(A) Quantification of mRNA levels of *Cebpβ*, *Pparγ*, and *Cebpα* at different differentiation time points using control cocktail (EtOH) or DHA cocktail (DHA). We observe significant DHA-dependent transcriptional activation of *Pparγ* and *Cebpα* within 24h of differentiation, but not of CEBPβ.

(B) A PPARγ-T2A-GFP knockin reporter generated using Crispr/Cas9 shows increased expression of PPARγ in response to DHA cocktail (DHA) compared to control cocktail (EtOH) within 3 days of differentiation. Addition of the FFAR4 antagonist AH7614 inhibits PPARγ expression in a dose-dependent manner. Dotted line denotes media changes, images are taken every 2h.

(C) Immunoblot showing CEBPβ and CEBPα protein levels at different time points of differentiation using control cocktail or DHA cocktail. We consistently observe a DHA-dependent increase in expression of CEBPα, but not of CEBPβ.

(D) Immunoblot showing phosphorylated and overall levels of ERK, AKT, and CREB levels at different differentiation time points using control cocktail, DHA cocktail, or FFAR4 agonist (TUG891) cocktail. While there is activation of these adipogenic regulators during differentiation, this is not DHA-dependent, suggesting that cocktail components other than DHA, notably insulin, activate these adipogenic regulators.

(E) While ERK and AKT activation is not mediated by DHA, activation of these pathways is required for DHA-enhanced adipogenesis, consistent with the notion that cocktail components other than DHA activate these adipogenic regulators and this is required for adipogenesis.

(F) 3T3L1 cells lacking CTCF show only a minor, not significant growth defect. Cell growth was assessed using Essen IncuCyte Live Cell Imaging Analysis in normal growth media; images taken every 2h.

(G) Loss of CTCF does not affect adipogenesis induced by the historical DM (1 μg/ml insulin, 1 μM dexamethasone, 0.5mM IBMX). (H-I) Three different 3T3-L1 *Ctcf* knockout cells lines were generated by Crispr/Cas9 using 3 different sgRNAs. The cell line sgCtcf-1 was used in Figure 6F-G.

(H) All three lines show an adipogenesis defect in response to DHA cocktail.

(I) TIDE analysis describing genomic rearrangement of all three engineered 3T3-L1 sgCtcf cell lines.